Nederlands Instituut voor Onderzoek der Zee
NETHERLANDS INSTITUTE FOR SEA RESEARCH (NIOZ)

# The measurement of currents at sea.

# Mooring design and current meter data analysis.

**J.J.M. van Haren**

**Reader for lectures given at the UNESCO training workshop on observation and analysis of currents at sea, Doha, Qatar 1 - 9 November 1992.**

**NIOZ P.O. Box 59 1790 AB Den Burg The Netherlands**

**Tel. 31 - 2220 - 69300 Fax 31 - 2220 - 19674**

# Preface

These lecture notes contain most of the matter I will be teaching during the UNESCO training workshop on current meter observations and analysis. During the preparation of the manuscript I consulted most of the references listed below as well as several scientific papers. The references given provide introductions to several topics in oceanography and to data analysis. Some of them (Jenkins & Watts, 1968 and Godin, 1972) are very useful guides for the reader who wants to learn all of the fundamentals on data analysis.

These notes contain introductions and basic theory on currents at sea (Chapter 1) currents measurements (Chapter 2), moorings (Chapter 3) and data analysis (Chapter 4). At times they may seem somewhat abstract, but (part of) the theory will be applied during the practical stage of the workshop.

I would like to thank mr. Amin Meshal (UNESCO, Doha, Qatar) for inviting me to this workshop and Prof.dr. W.G. Mook (director NIOZ) for allowing me to accept the invitation. Mrs. Carmen Blaauboer tremendously helped me by typing these notes.

Hans van Haren

October 1992
Texel, the Netherlands

## Useful References

**(Chapter 1)**

Open University, 1989. *Ocean circulation.* Pergamon Press, Oxford, 238 pp.

Pond, S., G.L. Pickard, 1986. *Introductory dynamical Oceanography.* Pergamon Press, Oxford, 329 pp.

Tolmazin, D., 1985. *Elements of dynamic oceanography.* Allen & Unwin, Boston, 181 pp.

**(Chapters 2 and 3)**

Krause, G., 1986. *In-situ measurements and measuring techniques.* In: Sündermann, J. (ed.), Oceanography, subvolume V/3a of Landolt - Börnstein, Numerical data and functional relationships in science and technology. Springer Verlag, Berlin, p. 134-232.

**(Chapter 4)**

Chatfield, C., 1975. *The analysis of time series: theory and practice.* Chapman and Hall, London, 263 pp.

Godin, G., 1972. *The analysis of tides.* Liverpool University Press, Liverpool, 264 pp.

Jenkins, G.M., D.G. Watts, 1968. *Spectral analysis and its applications.* Holden-Day, San Francisco, 525 pp.

Schuremann, P., 1941. *Manual of harmonic analysis and prediction of tides.* Government printing office, Washington, 314 pp.

## Contents

# 1. Introduction to currents at sea

According to the Collins Reference dictionary, part Seas and Oceans,

> *Ocean currents may be defined as parts of a fluid body of water moving continuously in a certain direction.*

Certainly, a continuous flow of water appears to an observer who watches a river, but may be less clear when he or she observes an ocean from the beach, where (breaking) waves firstly will be noticed. Fluid motion in the ocean extends over a vast range of scales in time and space and is generated by a number of forces each acting on different scales. A classification of scales and hence of possible driving mechanisms for water movement is warranted.

Physical space is described by a vector $\vec{X}$ = (x, y, z) relative to the Earth. It is decomposed into three components of which (x,y) describe the horizontal plane. Water flow will be indicated by a velocity vector $\vec{U}$ = (u, v, w), with components along the space coordinates above. A typical record of the u-component measured by a current meter at a fixed location shows an erratic as well as a deterministic behaviour superimposed on a mean value as a function of time (Fig. 1.1a). Such a record does not contain fluid motions on scales smaller than the isntrument itself or its preset sampling interval (typically 10 min). Such types of motion are classified as "turbulence", three dimensional erratic water movements at cm and (less than) s scales, and high frequency "waves" that are periodic at much less than s-min scales.

If we display the same record as a function of frequency ("spectrum") instead of time, we see a smooth variation of (kinetic) energy, with large values at low frequencies for motions with long periods, together with occasionally occurring high energy contents at distinct frequencies (Fig. 1.1b). As by definition a discrete frequency represents sinusoidal behaviour in the time domain, these spikes represent (dominant) wave motion, such as tides, that are periodic once or twice a day, and can, strictly spoken, not be classified as currents. We will do so however, and talk about tidal and long wave currents. Such waves behave according to the relevant aspect ratio in the oceans, where the vertical length scale is much smaller than the horizontal scales. Thus,

> *Ocean currents have dominant horizontal scales ($u,v >> w$) and may be periodic (in time), but at tidal scales or longer.*

Typical values of horizontal ocean currents range from a few mm/s for deep ocean flows to several m/s for flows through narrow straits.

As is seen from the spectrum, classification of different types of currents within the range given above is to be made next. Note that a record of limited duration, a month say, does not "resolve" motions that are periodic at very long time scales of months - years. Such motions exist in the ocean and will thus be described, but appear in a lumpsed - together fashion in such a spectrum.

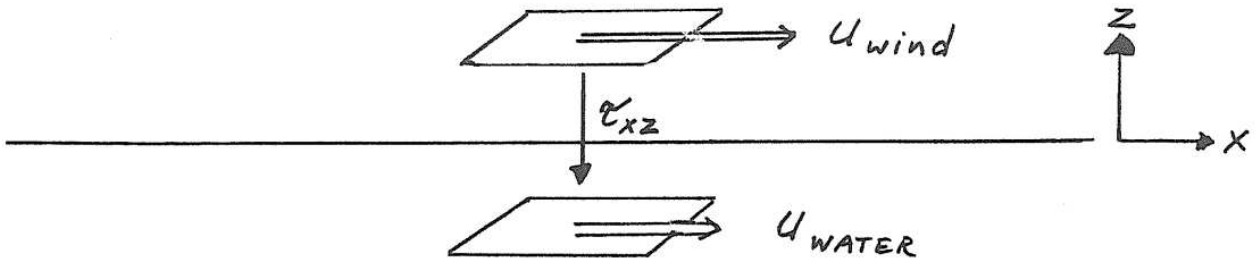


Fig 1.2 Transport of momentum from the wind blowing over the ocean's surface.

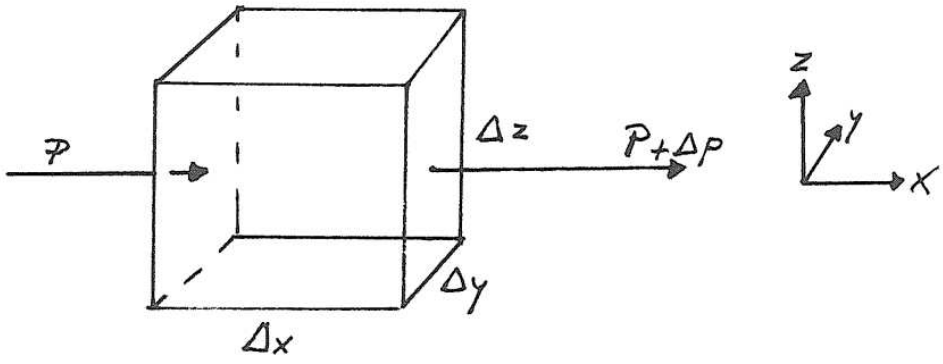


Fig 1.3

## 1.1 Description of ocean current generating forces

A change of current with time or acceleration is induced by a force per unit mass $F$ according to Newton's second law

$$\frac{d\vec{U}}{dt} = \vec{F} \qquad (1.1)$$

As in a system the ocean is coupled to the atmosphere and a considerable part of ocean currents is driven by their interaction.

A wind blowing over a sea generates drift currents via direct momentum exchange between the atmosphere and the ocean. This exchange is expressed in a drag or friction force

$$F_{Di} = \frac{-1}{\rho}\frac{\partial \tau_{iz}}{\partial z} \qquad i = x, y \qquad (1.2)$$

where $\rho$ is the density and $\tau_{iz}$ are components of the stress sensor (Fig. 1.2). It describes the action of an imaginary horizontal plate of air moving over the ocean's surface a so that it drags an imaginary horizontal plate of water with it via a vertical transport of momentum. Momentum is transported deeper into the ocean via internal friction expressed in the same form (1.2). This will lead to a vertical gradient in the current and (1.2) is expressed as

$$F_{Dx} = \frac{\partial}{\partial z} K \frac{\partial u}{\partial z}$$
$$F_{Dy} = \frac{\partial}{\partial z} K \frac{\partial v}{\partial z} \qquad (1.3)$$

where K is an exchange coefficient. It may be understood that at the sea floor, not moving relative to the water, frictional effects may retard the current, also expressed by (1.3).

A wind blowing in a constant direction also pushes the water to one boundary or coast of an ocean basin. This leads to wind set-up or a slope in the sea level. A sea level slope provides a pressure gradient that may drive a current. Another force that may generate sea level slopes is the tide generating force or the gravitational force of the Moon (Sun)-Earth system.

Imagine a cube of water of sides $\Delta x$, $\Delta y$, $\Delta z$ (Fig. 1.3). The pressure on the right side area $\Delta y \Delta z$ is $\Delta p$ higher than on left side of the cube. Then, in the x-direction a net force per unit mass is generated on the cube of the value $\frac{p\,\Delta x\Delta y - (p + \Delta p)\,\Delta x\Delta y}{\rho \Delta x \Delta y \Delta z}$ which in the limit of a small cube reads

$$F_{px} = -\frac{1}{\rho}\frac{\partial p}{\partial x}, \qquad (1.4)$$

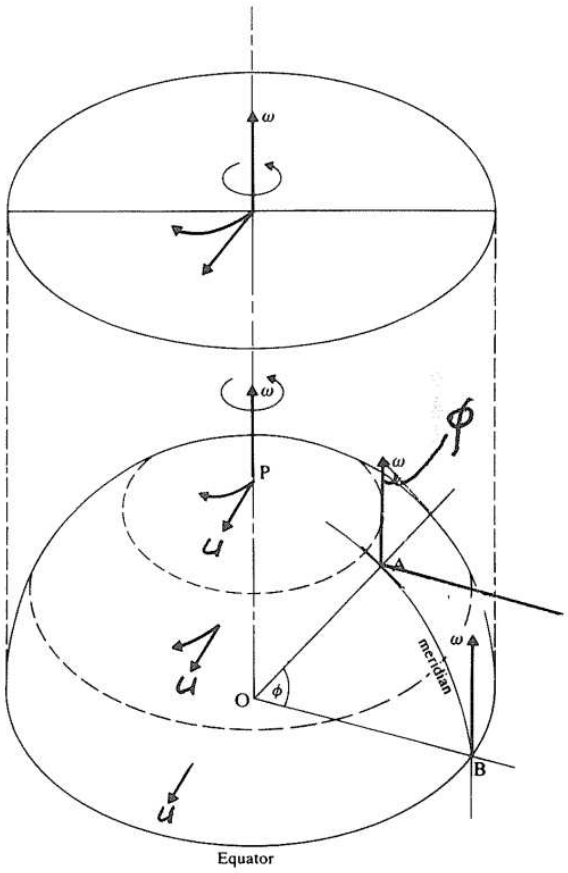


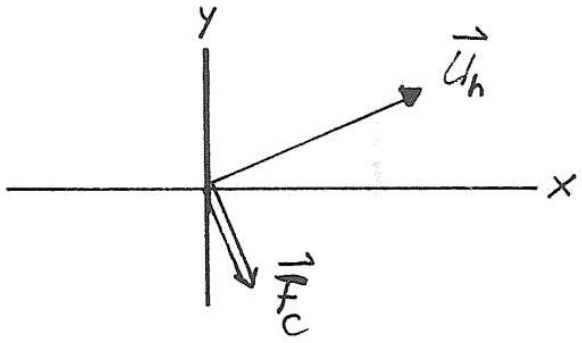


Fig 1.4 The change of Coriolis parameter $\omega \sin\phi$ with latitude and its deflecting effect on a particle moving on the Earth's Northern Hemisphere.

and similarly for the other two axes.

In the vertical direction another important force is imposed by gravity. As we are considering horizontal currents only, we neglect acceleration of the vertical velocity, which leads to the description of the vertical momentum equation as a balance of forces per unit mass, the hydrostatic balance

$$0 = -g - \frac{1}{\rho}\frac{\partial p}{\partial z}, \qquad \textbf{(1.5)}$$

where g is the acceleration of gravity. By integrating this equation from a vertical position z = z in the ocean to the sea level height z = ζ, we obtain

$$p(z) = p(\zeta) + \int_z^\zeta g\,\rho(z')\,dz',$$

so that the horizontal pressure gradient forces like (1.4) are decomposed as

$$F_{px} = -\frac{1}{\rho}\left\{ \underbrace{\frac{\partial p(\zeta)}{\partial x}}_{\textbf{(a)}} + \underbrace{g\,p(\zeta)\,\frac{\partial \zeta}{\partial x}}_{\textbf{(b)}} - \underbrace{\int_z^\zeta g\,\frac{\partial \rho(z')}{\partial x}\,dz'}_{\textbf{(c)}} \right\} \qquad \textbf{(1.6)}$$

and similarly for the y-direction. Term (b) in (1.6) shows that a slope or gradient in the sea level causes a pressure gradient force.

Equation (1.6) shows two other components of the pressure gradient force. Term (a) describes the sea level pressure gradient force that is caused by atmospheric pressure differences. Terms (a) and (b) are dependent of the horizontal coordinates (x, y), indicating that the currents they generate vary very in magnitude and direction in horizontal space, but they are independent of z. Such currents are called barotropic currents.

The density in term (c) is dependent of all three coordinates, and will generate currents that vary with depth, "baroclinic" currents. As the density of the ocean is mainly determined by temperature and salt content (salinity), as described by the "equation of state" of sea water, which shows that warm water is less dense than cold water and salty water denser than fresh water, the atmosphere has an indirect impact on ocean currents via this term. Heat and water (vapour) exchange between atmosphere and ocean generate density variations by cooling, warming and evaporation, precipitation.

An important force in the momentum equations is related to our non-inertial coordinates system, which is taken relative to the earth and hence rotating with it. A moving particle in such coordinate system is reflected from its path in a direction that depends on the sense of rotation of the coordinate system (Fig. 1.4). On the Earth's Northern Hemisphere it will be deflected to its right. The responsible force is the Coriolis force, which acts at right angles to the particles' path. The magnitude of this force depends on the magnitude of rotation of the coordinate system, which is a function of its latitudinal position on Earth, and it depends on the magnitude of velocity the particle is moving with. We write for the Coriolis force components

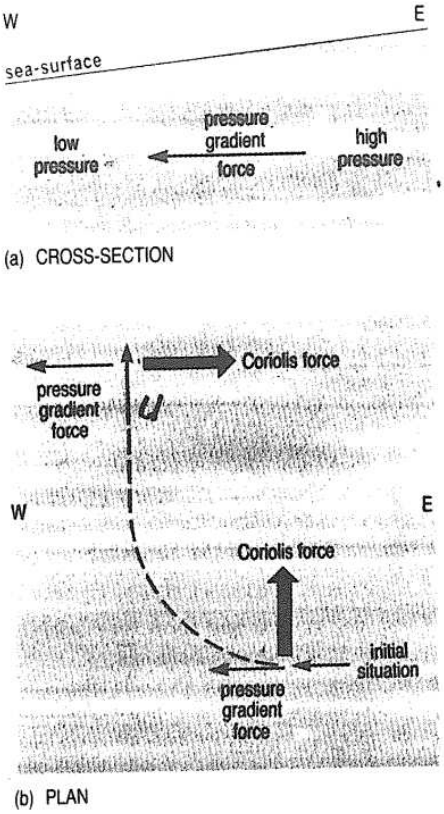


Fig 1.5 Geostrophic balance of a sea level gradient induced motion (u) in the Northern Hemisphere.

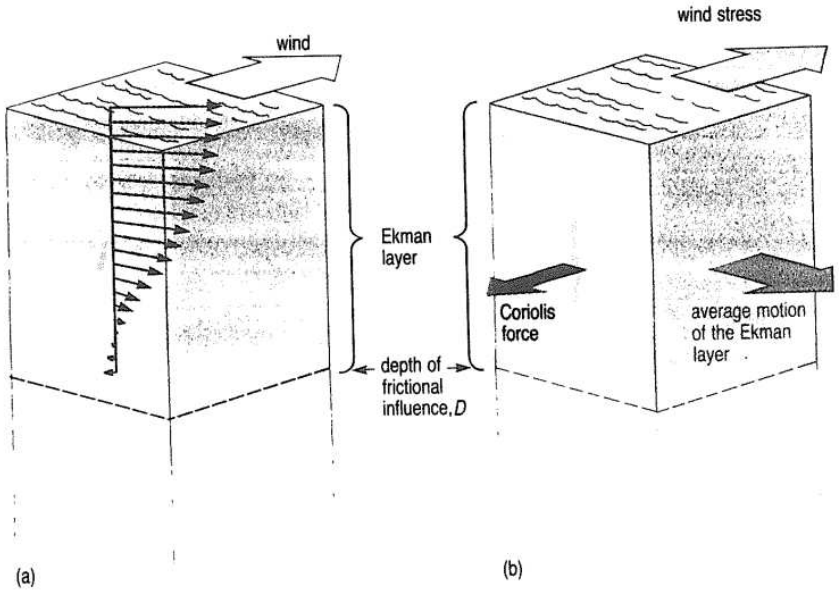


Fig 1.6 The wind-induced Ekman spiral of near-surface currents (black arrows).

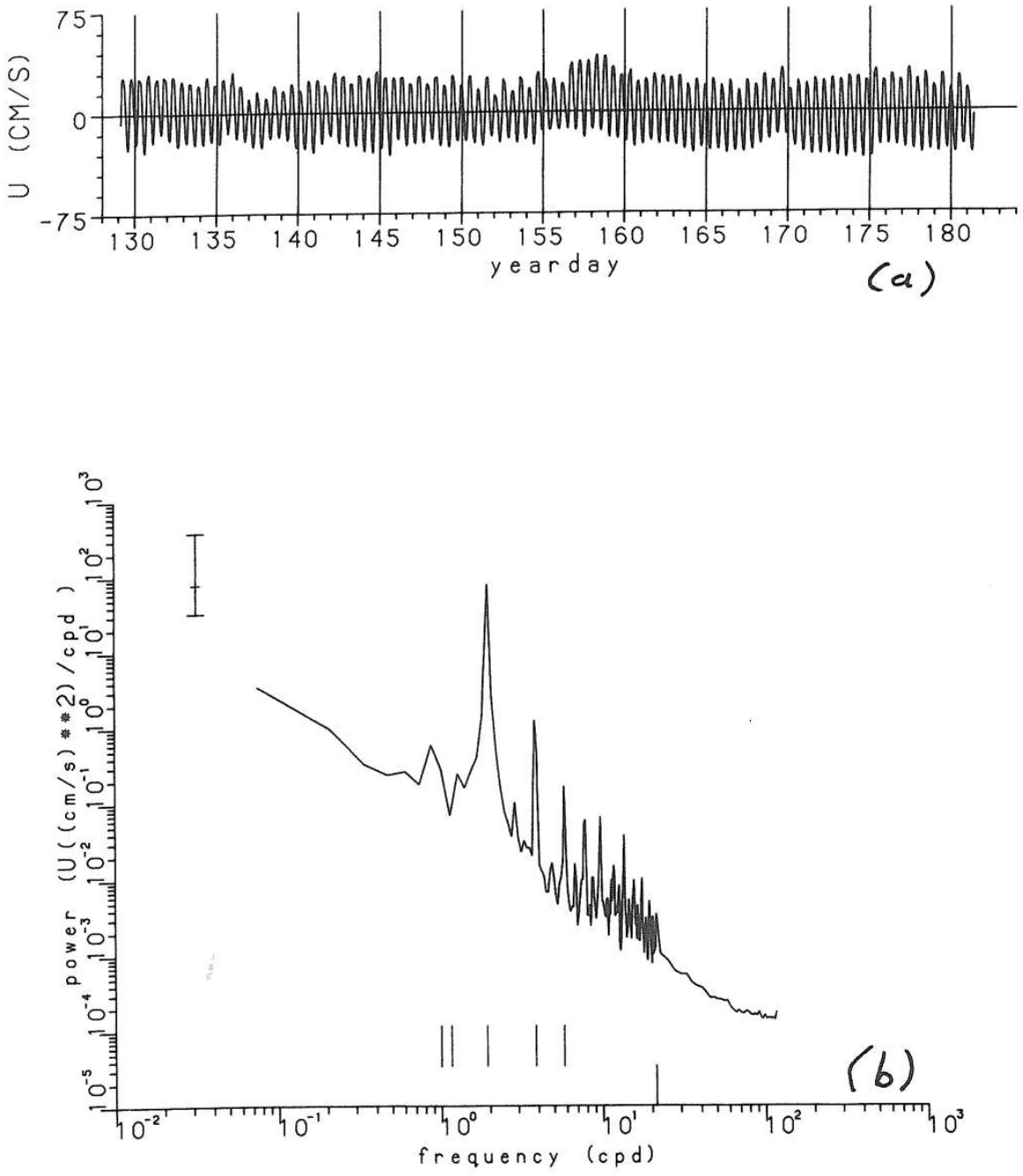


Fig 1.1 Example of a current meter record. PLotted are the u-component with time in days (a) and its spectrum with frequency in cpd (b).

$$F_{cx} = -f v \qquad F_{cy} = f u \tag{1.7}$$

where $f = 2\Omega \sin \varphi$ (for latitude $\varphi$ and angular speed of the Earth's rotation $\Omega$), the inertial or Coriolis frequency). At $\varphi \approx 25°$ (Doha, Qatar) we find with $\Omega = 0.729 \times 10^{-4}\ s^{-1}$, that $f \approx 0.62 \times 10^{-4}\ s^{-1}$.

Resuming we have the following set of equations that describe the momentum or currents per unit mass at sea

$$\frac{du}{dt} - fv = \frac{-1}{\rho}\left\{\frac{\partial p(\zeta)}{\partial x} + g\rho(\zeta)\frac{\partial \zeta}{\partial x} - \int_z^{\zeta} g\frac{\partial \rho}{\partial x}\,dz'\right\} + K\frac{\partial^2 u}{\partial z^2} + F_{au}$$

$$\frac{dv}{dt} + fu = \frac{-1}{\rho}\left\{\frac{\partial p(\zeta)}{\partial y} + g\rho(\zeta)\frac{\partial \zeta}{\partial y} - \int_z^{\zeta} g\frac{\partial \rho}{\partial y}\,dz'\right\} + K\frac{\partial^2 v}{\partial z^2} + F_{av} \tag{1.8}$$

(a) (b) (c) (d) (e) (f)

where K is a constant of 0 ($10^{-3}\ m^2/s$) $F_{au}$ and $F_{av}$ are additional forces, such as the tide generating force, which is important in the oceans only.

## 1.2 Balance of forces

For a description of most currents measured by current meters, a verification of the stationary (or non accelerating) current problem is sufficient. Term (a) in (1.8) is considered small. If we neglect frictional effects, term (f), we find a balance between the Coriolis and the pressure gradient forces, the "geostrophic" balance. This is the main balance in the ocean, outside frictional boundary layers. Under this balance water is moving at right angles to the pressure gradient instead of moving down it(Fig. 1.5).

Near frictional boundaries a balance between the frictional and Coriolis forces is important. At the turn of this century Ekman developed the theory of wind driven currents in order to explain Nansen's observation that ice movements in response to wind were at an angle to the right of the wind. Ekman assumed a homogenous ocean with a horizontal sea surface and found from the balance above that at the sea surface the current deviates 45° from the wind direction. This angle increases with depth, whereby the current magnitude exponentially decreases due to friction. A spiral pattern results (Fig. 1.6). The "Ekman" depth over which the wind influence is felt is

$$D_E = (2K/f)^{1/2}$$

whichi is of O(10 m) typically. In this layer the average motion is at right angles with the wind and the Coriolis force is opposite to the it. The average velocity magnitude in this layer is given by $|U| = \tau / D_E f \rho$ where $\tau$ is the wind stress. For typical values of $K = 10^{-2}\ m^2 s^{-1}$ and $\tau = 0.1$ N (wind velocity of 5 m $s^{-1}$) we find $D_E \approx 18$ m (Doha) and $|U| = 9$ cm $s^{-1}$.

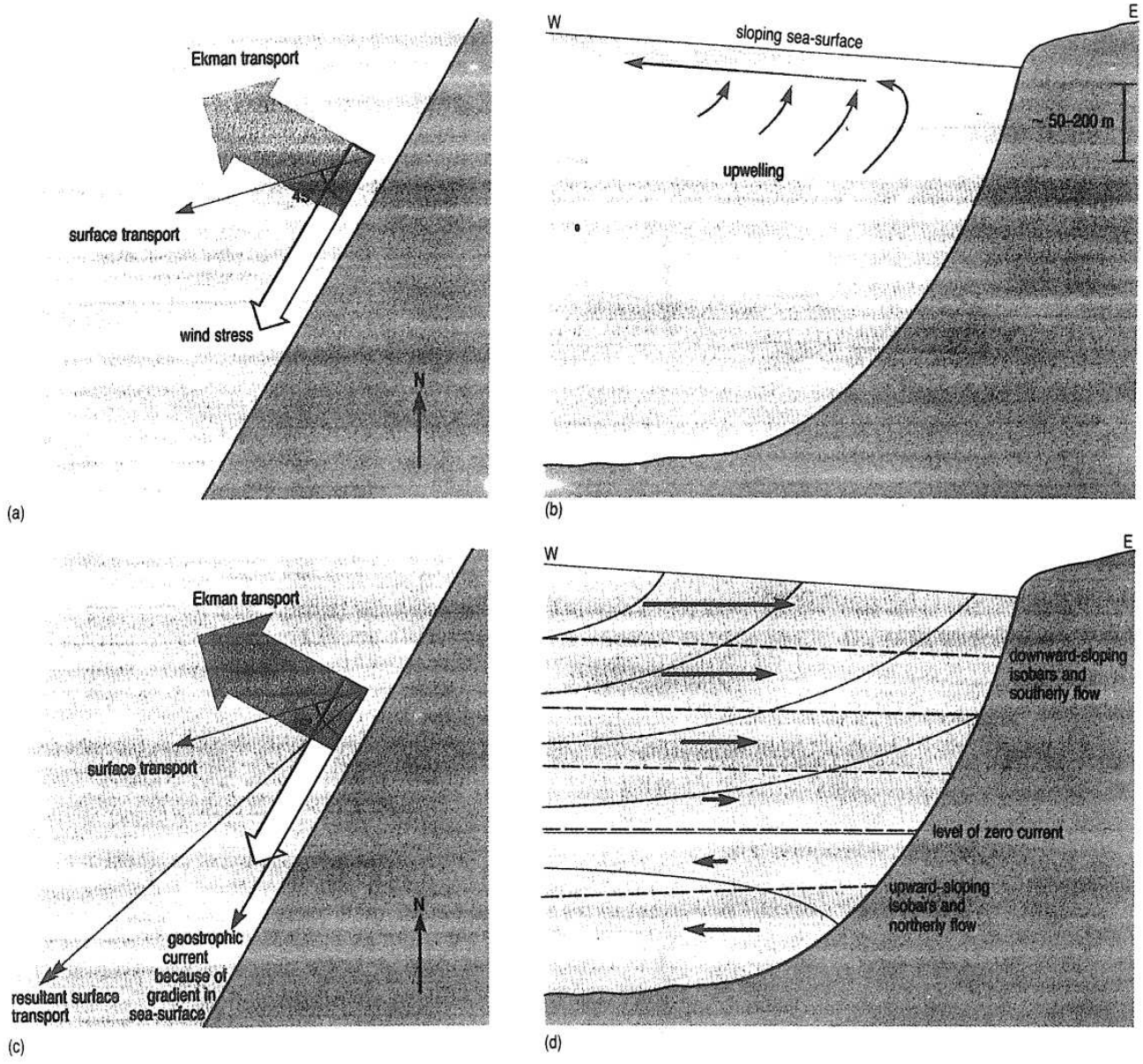


Fig 1.7 Dynamics induced by wind blowing along a coast (plan views a,c and cross-sections b,d). In the initial stage surface Ekman transport is directed off-coast (a). This causes a sea level slope (b), which is geostrophically balanced (c). In a stratified sea a near-bottom counter-flow is formed due to baroclinic and bottom boundary effects (d).

A similar Ekman spiral may be found near the ocean's bottom over which water is in motion. Here the spiral is directed to the left of the undisturbed flow. In shallow seas the surface and bottom Ekman layers overlap, resulting in a wel-mixed water column.

When the wind that has been driving a current suddenly ceases to blow another interesting motion is found in the deep ocean, where frictional forces may be small. The Coriolis force acts as a centripetal force and a curved motion results. The path of this inertial current will be circular if the motion involves only a small change in latitude. Its frequency is the inertial frequency f.

Although processes leading to currents can be quite complex, most of the measured ocean currents can be explained by a geostrophic balance. As an example consider a lateral boundary with wind blowing along it (Fig. 1.7). The wind drives an Ekman transport off the coast, causing the sea level to slope. The currents generated by the sea level gradient will be deflected by the Coriolis force. In equilibrium, a geostrophic balance results for the along-shore current.

## 1.3 Examples of ocean current systems

The Sun drives the "general ocean circulation" the ocean's climate. It warms the oceans more at the equator then at the poles, and causes an inhomogeneous evaporation - precipitation distribution across the oceans, with the former dominant in the Northern Hemisphere. In the ocean's surface layer the flow driven by the resulting pressure gradient and deflected by the Coriolis force takes the shape of two oppositely rotating gyres on each Hemisphere (Fig. 1.8).
The climatic winds, also driven by the Sun, simply modelled by easterlies at mid-latitudes and westerlies at low-latitudes, generate a flow pattern that adds positively to the circulation above. The current values of a few mm $s^{-1}$ - cm $s^{-1}$ are enhanced to O(10 cm $s^{-1}$ -1 $ms^{-1}$)in localized areas such as the Equator. Due to the meridional (frictional) boundaries and the rate of change of the inertial frequency with latitude, the circulation becomes asymmetric with intensified currents near western boundaries. These currents, with the Gulf Stream as example, may be viewed as huge rivers, with characteristic current values up to 2 m $s^{-1}$!

At greater depth currents do exist, although they are weak away from boundaries. The differential heating with latitude results in sinking of cold water near the poles and upwelling near the Equator and thus generates a meridional heat transport much like the one in the atmosphere. The three-dimensional circulation in the ocean is more complex, however, with salinity and temperature contributing their shares to density.

In shallow seas the climate of currents is determined by the ocean, if they are bounded to it, and by direct atmospheric influences via prevailing winds. In the Persian Gulf the most probable mean circulation is driven by density differerences, with evaporation in the shallow Gulf areas causing dense salty water to flow out of the Gulf along the southern coast and fresh Indian Ocean water flowing into the Gulf near the Coast. The prevailing North-westerly winds enhance the near-surface inflow along the Northern Coast (Fig. 1.9).

On smaller time scales winds may vary considerably and thus impose variations in the general circulation schemes. On a seasonal scale (Monsoons) they may

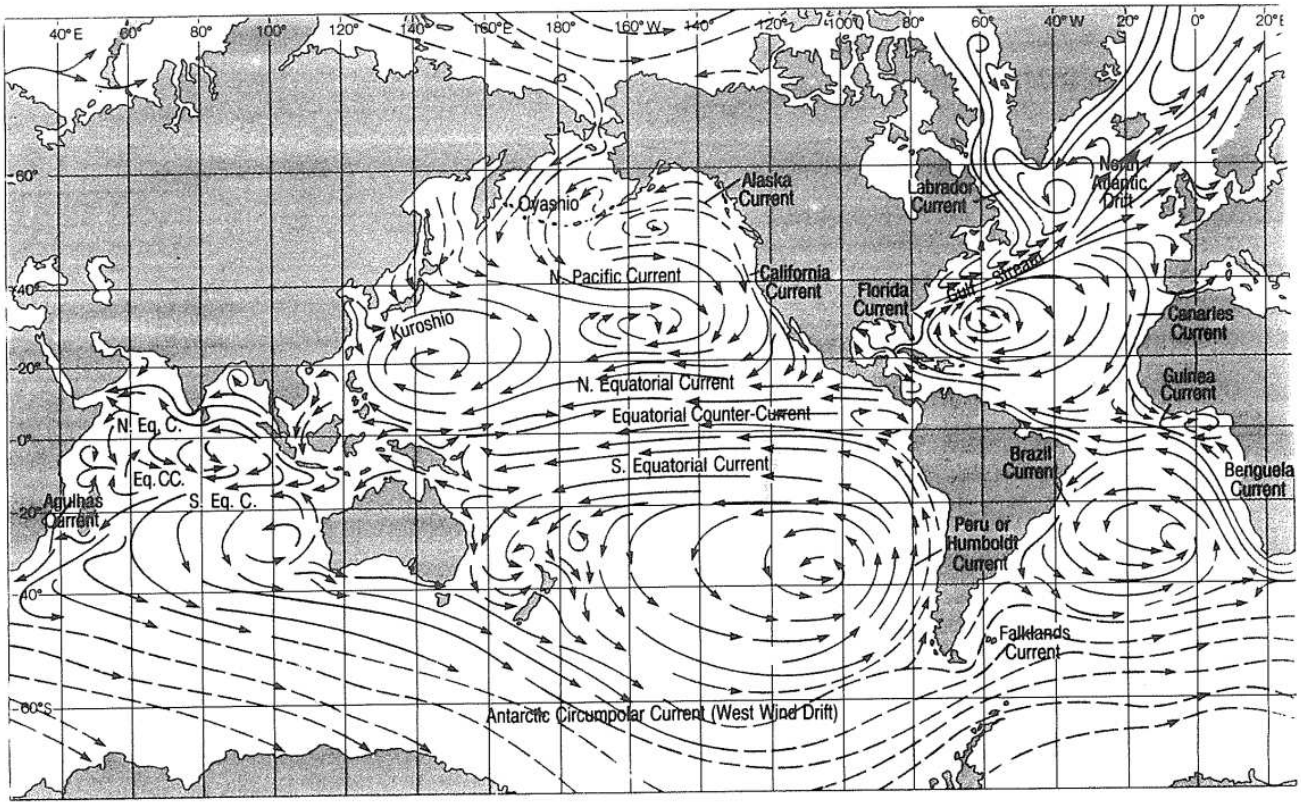


Fig 1.8 The global ocean surface circulation. Cool currents are indicated with dashed arrows, warm currents by solid arrows.

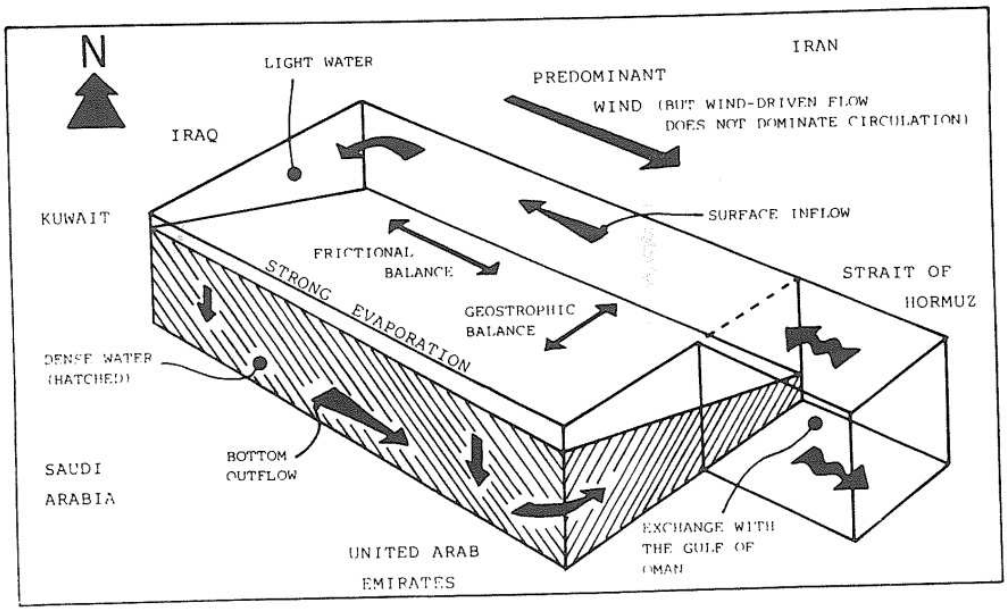


Fig 1.9 The probable circulation pattern in the Persian Gulf.

affect large ocean areas and on "synoptic" scales of mid-latitude low-pressure systems they affect areas of the size of the Gulf.

Atmospheric low-pressure systems have a quasi-geostrophic cyclonic circulation. Such gigantic gyres or eddies may also be found in the ocean where horizontal gradients of currents are encountered, such as at the boundaries of the Gulf Stream. Internal frictional layers cause the line of horizontal density gradients "front" to adopt a wave ("meander") that may become unstable. Growing instabilities may end up as eddies that may leave the Stream. Gulf Stream eddies have sizes of O(100 km), and may fool an observer who measures currents at a fixed position as they are advective past that point. The time series will show a wave at relatively long periods (dependent on the size of the eddy and the advectex speed) not related to the nature of the eddy, which in time is relatively persistent.

Similar effects due to the wind may show up in time series. A current meter fixed near an ocean front may find enhancement of currents at synoptic scales due to advective displacement of the position of the front by passing atmospheric disturbances.

On smaller spatial scales quasi persistent complex flow patterns are found near river interface outflows, where a sharp fresh-salt water interface is encountered. Both lateral and bottom topographic inhomogeneitics cause local intensification of flow. Shoaling of the water column will increase the current velocity proportionally through continuity and a constant flow past a headland creates eddies in its wake (Fig. 1.9.6).

Several long periodic large scale wave types exist. Here we resume only with the energetically most important ones: tides.

Gravitational forces in the Earth-Moon and Earth-Sun system generate tides, which have two major periods due to the position of the Earth's rotational axis: diurnal and semidiurnal. Depending on the position on Earth one of the two or a combination dominates data records (Fig. 1.10). These periods differ from the typical atmospheric time scales and hence tides may be separated fairly easily from other types of currents. Only in the ocean the tide generating force directly generates (weak) tidal currents. The tide in shallow seas is generated via their oceanic boundary through sea level differences. The dimensions of a basin may drive the tide to or out of resonance and hence tidal currents may be weak (cm $s^{-1}$) or strong (m $s^{-1}$). The Coriolis force also affects tidal currents. In the horizontal plane particles follow an elliptic path (Fig. 1.11). Its ellipticity may vary from o (linear shape) to 1 (purely circular motion) due to lateral boundaries and frictional effects near the bottom.

So far we considered barotropic tidal currents generated by sea level variations. An internal horizontal density interface may act as a (tidal) wave guide as well. Internal tides are generated via interaction of the barotropic tide with bottom topography, amongst other forcing mechanisms. As their waveguide has different characteristics like than the sea surface in terms of vertical density differences, internal tides have different characteristics phase speeds and vertical current structure compared to barotropic tides (Fig. 1.12). This enables the observer to distinguish internal tidal currents, that may reach values similar to those for barotropic tides, from barotropic tidal currents, provided some spatial coverage is obtained by using multiple instruments and moorings. A single point current

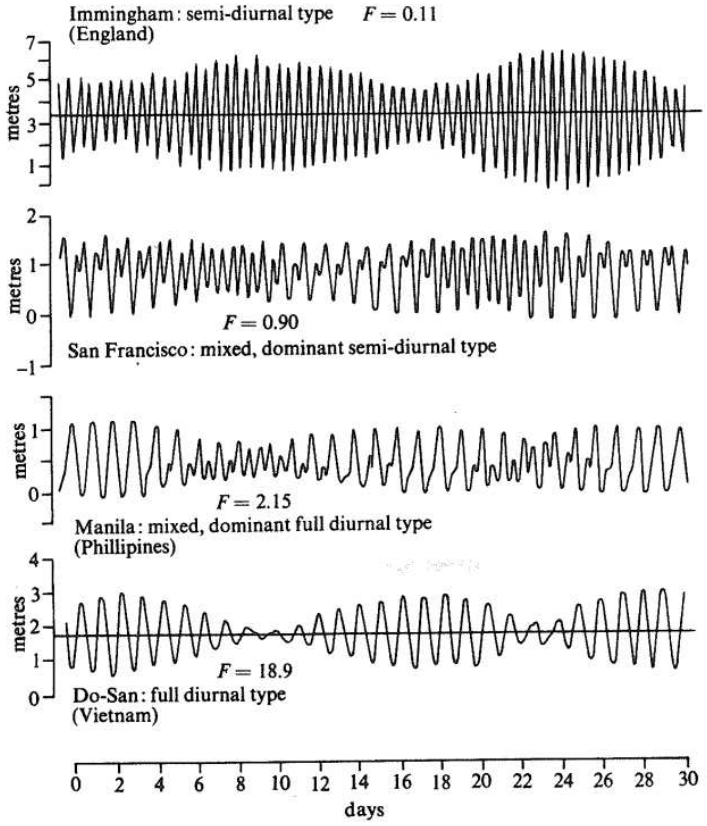


Fig 1.10 Examples of tidal observations.

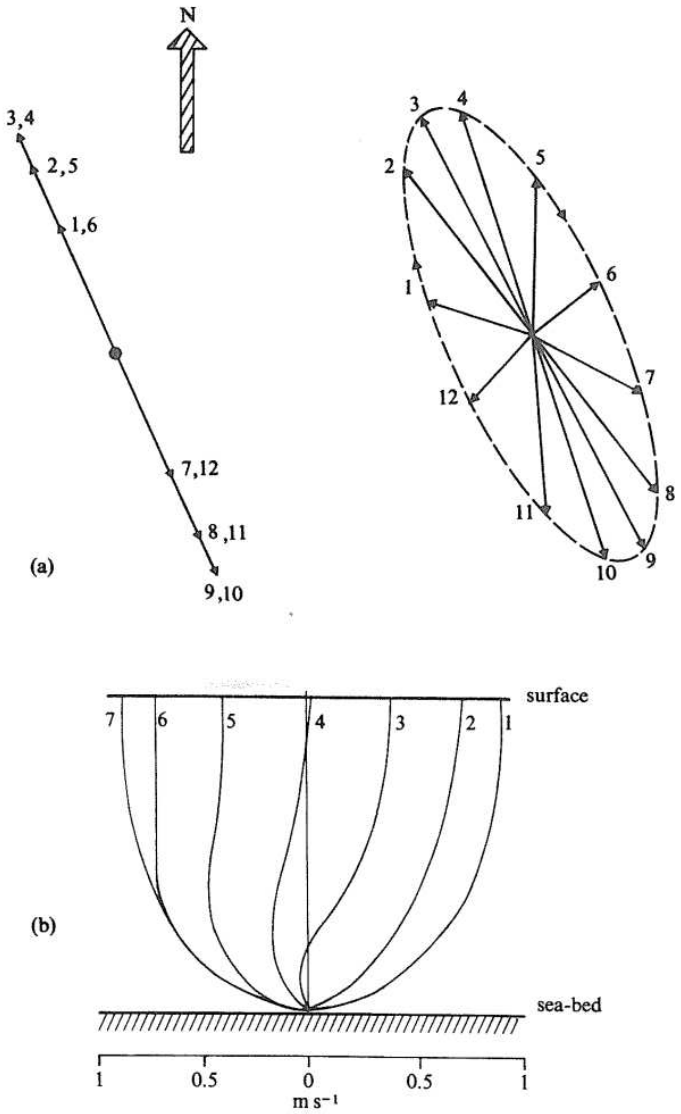


Fig 1.11 Examples of tidal currents. Ellipses of the current vector in the horizontal plane are drawn as a function of lunar hour (a). Vertical tidal current structure in a shallow sea is shown in (b).

meter record from a stratified sea may provide rather erratic estimates of barotropic tidal currents due to the varying intensity of internal tides cuased by the internal density interface which generally is not persistent in time.

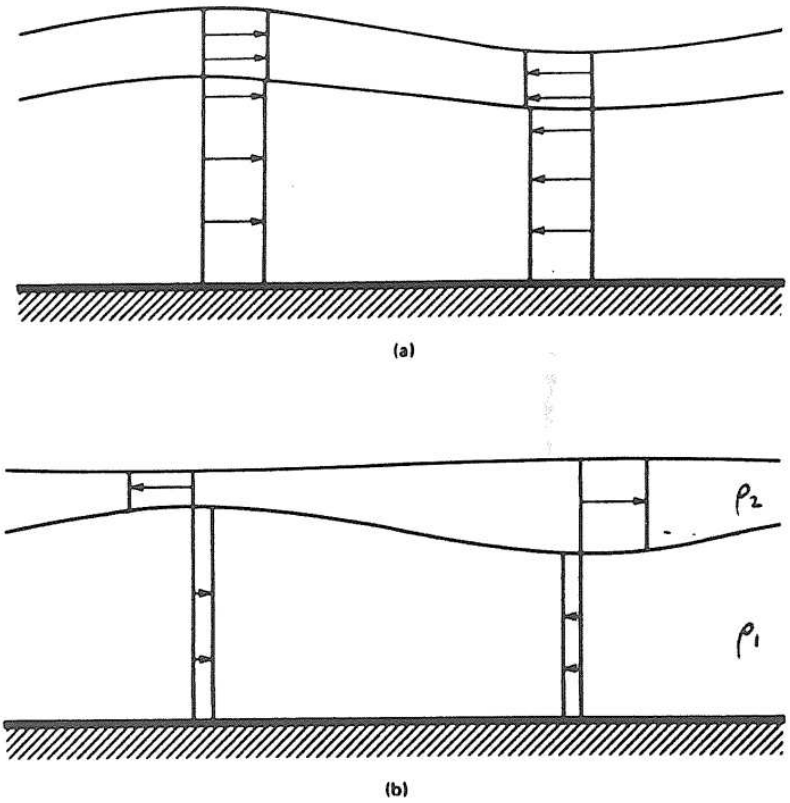


Fig 1.12 The relative velocities in a two-layer system ( $\rho_2 < \rho_1$ ) for a barotropic wave (a) and a baroclinic wave (b).

# 2. The measurement of currents at sea

In Chapter 1 we defined currents at sea and learned that even under the given definition a wide range of space and time scales are to be resolved by the measurement of water velocity. A choice of the process or current one wants to observe will lead to a choice of resolvable scales and hence the type of observational technique. There are many methods for measuring currents, but they all fall into one of two basic groups, direct and indirect methods. Two major categories of direct methods can be recognized.

Firstly, we describe the Lagrangian, or drift, direct method. Defining the velocity of a fluid element as

$$\vec{V}(t, \vec{a}) = \frac{d\vec{X}(t, \vec{a})}{dt} \qquad \text{with } \vec{X} = \vec{a} \text{ al } t = t_o \qquad \textbf{(2.1)}$$

from which we see that a water parcel, moving relative to the Earth (coordinates $\vec{X}$), is followed along its trajectory by an observer who records its position as a function of time t. The velocity is determined from the particles' change of a position with time along its trajectory.

Secondly, one could measure the flow past a fixed position relative to the Earth as a function of time. One then obtains directly estimates of the Eulerian flow velocity

$$\vec{U}(t, \vec{X}) \qquad \text{with } \vec{U} = \vec{U}_o \text{ at } t = t_o \qquad \textbf{(2.2)}$$

where the current vector $\vec{U}$ = (u,v,w) is composed of three components along the Cartesian coordinates $\vec{X}$ = (x, y, z).

The two definitions of current velocity are difficult to relate. It is seen that the two methods yield equal results only for stationary flows.

Finally, indirect methods involve measuring some property other than the motion of the water, from which the motion can be deduced. Two types of property may be considered suitable: those responsible for causing the current, like pressure differences and wind stress, and those that result from the currents, like the density distribution. We have seen that these two categories are often indistinguishable, e.g. density in turn determines the pattern of currents and assumptions on a balance have to be made.

## 2.1 Lagrangian current measurements

For Lagrangian methods, positions must be very accurately located at successive intervals of time. A major problem is to find an object that will move with the water and that can be satisfactorily tracked. Large objects that can be tracked visually or by radar, or by monitoring radio or acoustic signals which they emit, cannot respond to small-scale movements. Only large scale quasi Lagrangian flows can be measured.

Vessels on passage normally fix their position with navigational instruments at certain time intervals like once every 24 hours. Between the fixes dead reckoning, a method of estimating position from a knowledge of the course

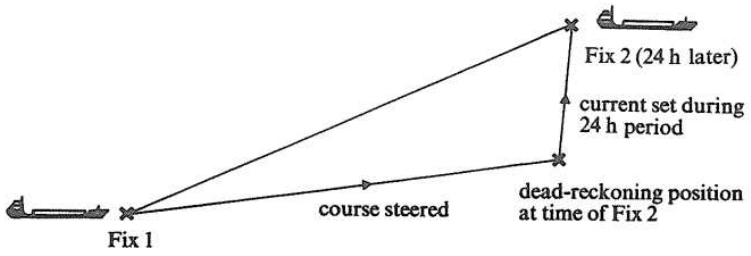


Fig 2.1 The assessment of mean current during a 24 hour period, as determined from a ship's drift.

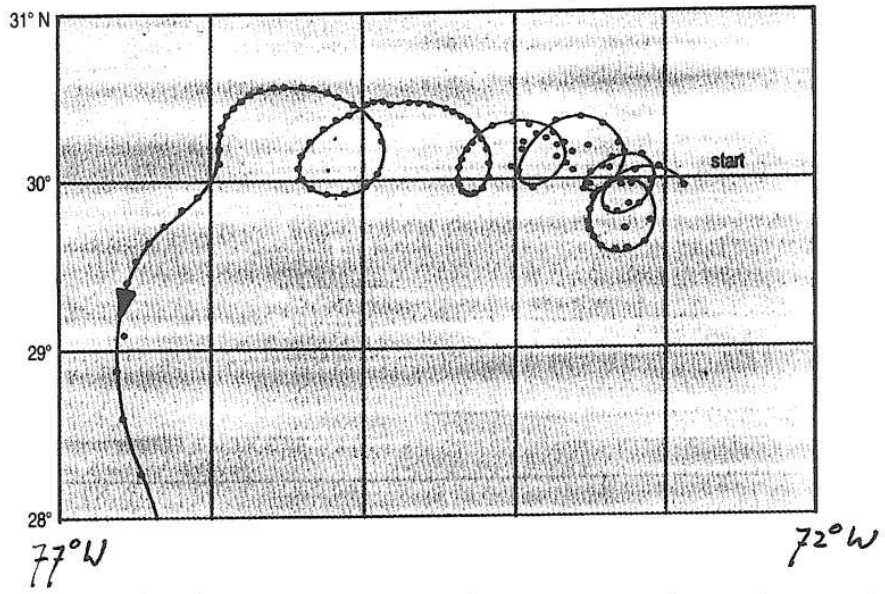


Fig 2.2 The path of a SOFAR float, with dots showing daily positions. Note the eddy (speeds: 0.5 m/s).

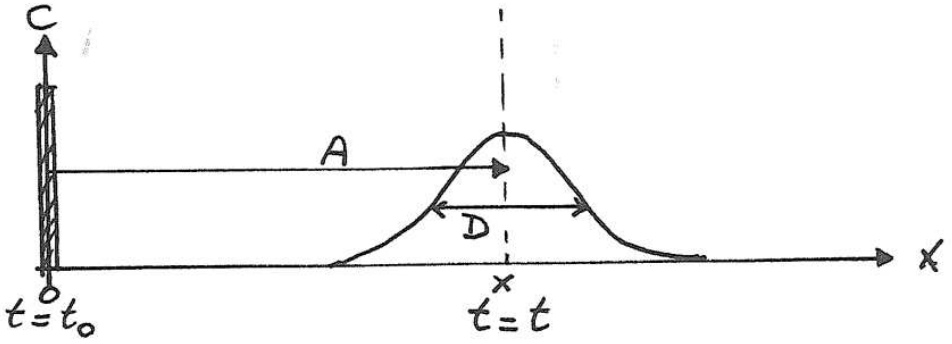


Fig 2.3 Particles released at t=t0 at position x=0 will be advected (A) to position x=x and spread apart by diffusion (D) by ocean currents over time t. Concentration = C.

steered and the speed maintained, is used to keep a continuous record of position. The accumulated discrepancy between the dead reckoning position after 24 hours, and the true position is an indication of the average displacement of the surface layer of water through which the vessel has passed (Fig. 2.1). Naturally, strong winds may bias the estimates of the true water velocity. Other problems are caused by surface waves, in keeping the intended course, and the accuracy of the navigational equipment.

Near-surface currents can also be studied with so-called parachute drogues - parachutes in the water rigged to be moved by currents, the drogue being attached by a thin line to a light surface float that can be tracked by a ship. With the more recent development of neutrally buoyant floats, current movements can now be determined at intermediate depths. In their simplest form these floats consist of aluminium tubes, equipped with acoustic transmitters. The tubes are ballasted to be just negatively buoyant at the surface, so that initially they sink. However, as they are less compressible than water, their density increases more slowly with pressure (and thus depth) than does the density of seawater. At some intermediate depth in the ocean they thus become neutrally buoyant and then move with the water at that depth. The acoustic transmitters enable surface vessels to track the floats without their having any attachment to the sea-surface, and of course they are not subject to the direct effects of wind. Systems have also been devised to track neutrally buoyant floats in the sound channel, a depth zone in the ocean over which the velocity of sound is relatively low so that it acts as a sound waveguide, from shore-based stations, and to enable one vessel to monitor the positions of many floats. The complex movement of currents at intermediate depth that can be revealed by this method is illustrated in Figure 2.2. Also, Argos buoys transmit signals to shore-based stations via satellites and can thus be tracked in remote oceans.

In shallow coastal waters, currents near the sea-bed can be charted by the movements of drifters that are just negatively buoyant and so trail along the sea-floor. Sea-bed drifters and the layer of water in which they are moving, however, are subject to frictional influences and hence their movements cannot be taken to represent that of the main body of water above.

A release of a large number of small drogues or trackable material provides estimates on the spread of water parcels. This spread can be expressed in a diffusive part, due to the turbulent or chaotic movement of water and an advective part due to the larger scale current (Fig. 2.3)

An old method to measure the integral effect of such flow is the release of bottles. Recently, an accidental release of Nike shoes resulted in a report on the general circulation in the Pacific Ocean.

Accidental or intended releases of chemicals have been used in the recent past. Such materials should be "conservative" in the sense that their concentration is little affected by non-flow conditions like chemical reactions, at least not in an unpredictable manner on time scales of the order of the period of observations.

Examples of accidental releases are oil spills that can be used to estimate near-surface currents. Releases of radio-active waste from Cap la Hague (France) and

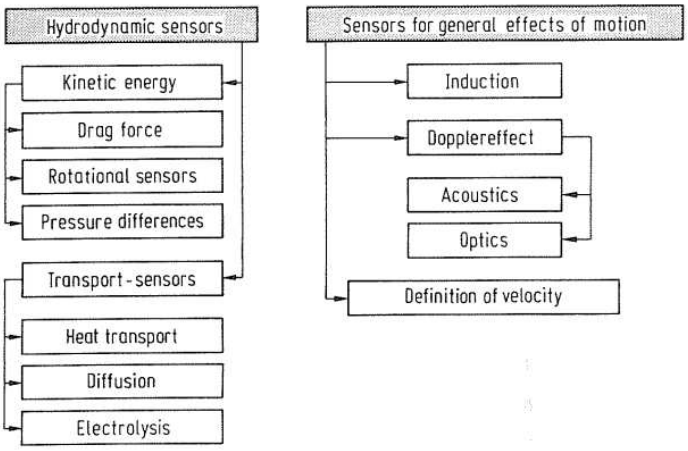


Fig 2.4 Principles of Eulerian current measurements.

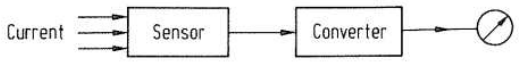


Fig 2.5 Flow diagram of current meters utilizing the kinetic energy of fluid flow.

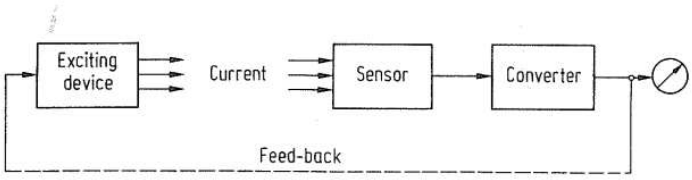


Fig 2.6 Flow diagram of current meters utilizing general effects of motion.

Sellafield (UK) have been used to map the circulation on the North-West European Shelf.

Radio-active labelled particles as well as strong colorants (Rhodomine B) have been used in planned experiments. The development of highly sensitive instrumentation led to the lowering of detection limits so that a very small amount of suitable chemicals is needed to map out a vast area at sea.

Finally, natural discharges of material like sediments or phytoplankton may be tracked. Here, the use of satellites has facilitated the recognision of flow patterns tremendously.

## 2.2 Eulerian current measurements

Generally, the data obtained from Langrangian measurements cover large ocean areas, but provide a course temporal resolution. Eulerian measurements provide better resolution in time, but they are moored in fixed positions. If one wants sufficiently long time series of data, instrumentation that will be described shortly is especially subject to unfavourable environmental conditions.

Sea water is a very corrosive fluid. The outmost care with the choice of materials for instrument housings and sensors is of vital importance for succesful measurements. The same holds for an array of instruments in a mooring.

High hydrostatic pressure is a factor which prescribes to build containers for electronic circuits as small as possible, and it has to be taken into account for the protection of pressure-dependent sensor elements.

Shock and vibration are further characteristics experienced by under-water instrumentation. The mechanical wear and tear on mooring and instruments in the reach of orbital wave motion determines greatly the lengths of time series to be measured in the upper layers of the ocean.

Fouling of sensors by marine growth in the euphotic zone is a great problem, particularly in the warm water sphere and during particular summer months in the moderate latitudes.

By the rapidly advancing use of low-power integrated circuits including solid state memories for data storage, the power supply of self-contained instruments poses less problems than before. Nevertheless, further development of suitable batteries for extensive periods of measurement at low temperatures is still desirable.

We describe two types of Eulerian current sensors (Fig. 2.4). Firstly, sensors are discussed which utilize the kinetic energy of fluid motion and transport properties of currents. The basic flow diagram of respective current meters is sketched in Fig. 2.5. The equations for momentum and transport involve physical properties of the fluid. Consequently, measurements by sensors based on these equations must depend on these properties as well. In principle, readings obtained by sensors will depend on density, i.e. on temperature and salinity, and on transport coefficients in the case of transport sensors.

Most of a second class of current meters, which utilize general effects of motion, like induction or Doppler effect, need an exciting device to generate magnetic fields, sound waves or light. Their basic flow diagram is presented in Fig. 2.6.

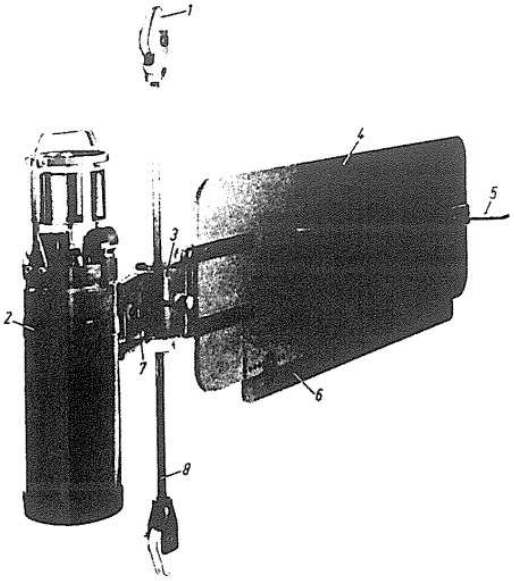


Fig 2.7

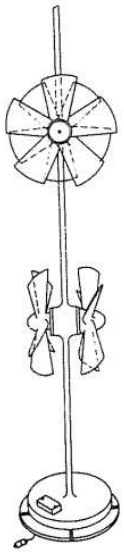

Fig 2.8

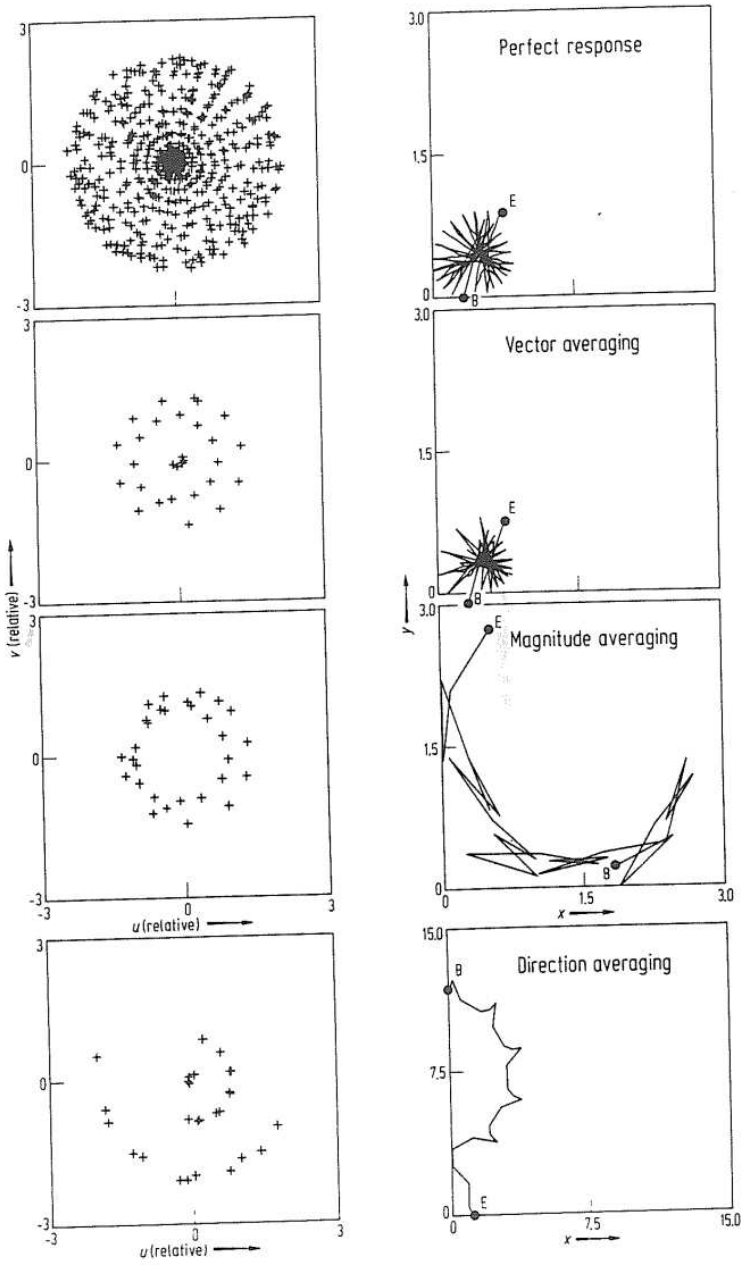


Fig 2.9

### 2.2.1 Current meters with hydrodynamic sensors

Current meters of this kind are the ones that we will be using during this workshop. In response to currents some kind of rotor mechanically rotates about an axis due to an asymmetric distribution of resistance. They possess a moment of inertia and they are subject to friction in their bearings. One of their disadvantages is that they cannot measure infinitely small velocities and starting velocities of 2-3 cm/s are most common. Another disadvantage of rotating elements is that a certain amount of water, dependent on the time constant of the instrument, must have passed the rotor before it has adjusted to a sudden change in the current velocity.

In addition to the rotor a vane is used for direction. It measures direction by reading a compass, after adjusting the instrument in the mean current (Fig. 2.7). The number of rotations that are read at time intervals provide the integral current magnitude. The compass is read optically or with a potentiometer giving the current direction at discrete time intervals. Although meters exist that measure the two horizontal velocity components directly by two orthogonal cosine response propellors (Fig. 2.8), current meters described above are used most commonly.

The time intervals over which the current is measured is usually shorter than the preset intervals at which the data are stored internally. Some current meters average current magnitude and direction. It may be shown by single vector analysis that this is wrong and leads to large errors when the current direction changes a lot over the time interval. One should average the velocity components. This is done by a vector averaging current meters, (VACM). A test series shows that especially erroneous estimates of the long term average, or residual, currents are generated by improperly averaging (Fig. 2.9).

In case of strong lateral turbulence or under the action of orbital motion like induced by surface waves, a combination of a large vane and, especially, an omnidirectional Savonicus rotor yields a grossly overestimated mean current. To be safe and to avoid additional erroneous measurements due to mooring vibrations (Chapter 3), one should avoid the use of current meters sketched above within the upper 10-15 m of the water column.

The displacement of a solid body hanging freely in a current provides measurement of the drag force $F$. In a stationary current this force is related to the current by

$$F = \tfrac{1}{2} C_D \rho A |\vec{U}| u \qquad (2.3)$$

where $C_D$ is the instruments' drag coefficient, $A$ the cross sectional area of the body (perpendicular to the current direction or the total area depending on the shape), $\rho$ the fluid density and $|\vec{U}| = (u^2 + v^2 + w^2)^{1/2}$ the current magnitude. Examples of such sensors are shown in Fig. 2.10. These instruments too, are sensitive to shallow water waves and can not be used near the surface. They especially require sensitive tilt sensors.

Along the same line one could measure the hydronamic pressure $P_h$ with a Pitot tube,

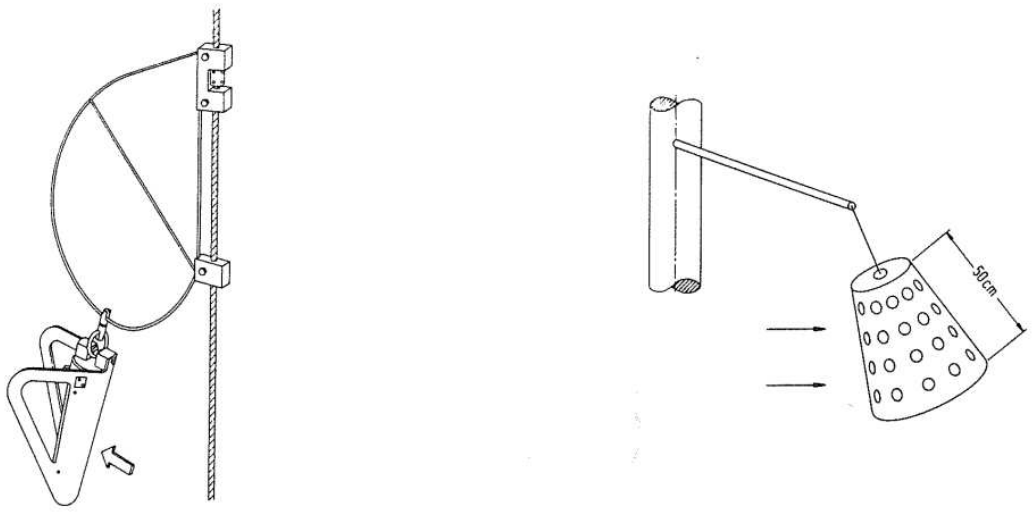


Fig 2.10 Examples of drag force current meters.

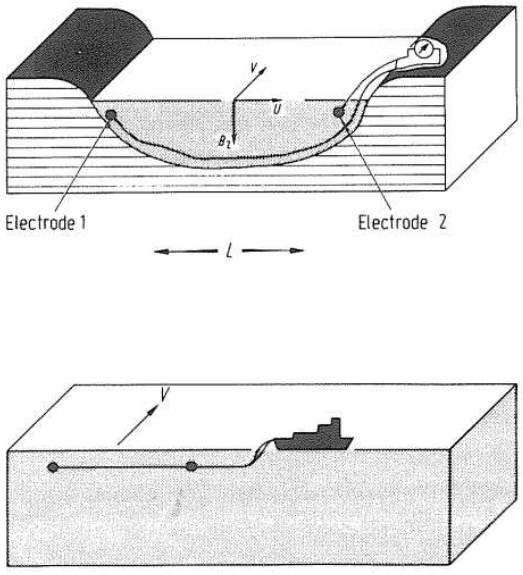


Fig 2.11 Geomagnetic current measurements of flow through a Strait (upper) and perpendicular to a ship's course.

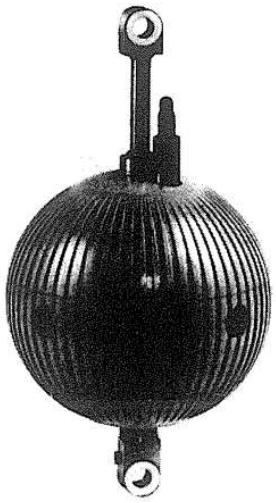

Fig 2.12 Self contained electromagnetic current meter.

$$P_h = \tfrac{1}{2}\,\rho\,|\vec{U}|^2 . \qquad (2.4)$$

Within the range of velocities in the ocean, the pressures (2.4) are very small and only high performance differential pressure sensors can be used. This principle has had only a few applications in the ocean so far.

A rod or wire heated above ambient fluid temperatures can measure the water velocity by adjusting either its resistance (temperature) or its current to constant values under the cooling effects of the (fluctuating) flow. Such heat transport sensors are quite commonly used in the laboratory to measure fast (turbulent) velocity fluctuations. In order to achieve small response times, it is necessary to use very thin and short sensors. This poses difficulties for the use in the corrosive marine environment, with additional problems due to fouling by plankton, dirt and air bubbles and they are not commonly used in moorings.

### 2.2.2 Current meters based on the general effects of motion

When an electrolyte moves with velocity $\vec{U}$ through a magnetic field of flux density $\vec{B}$, an electrical potential gradient $\vec{\nabla}\varphi$ is generated, which causes an electrical current density $\vec{i}$ depending on the conductivity $C$.

$$\vec{\nabla}\varphi = \vec{U} \times \vec{B} - \frac{1}{C}\vec{i} \qquad (2.5)$$

Because of the presence of the Earth's magnetic field any ocean current generates potential differences which may be measured to derive the speed of moving sea water. Although the interaction of hydrodynamic and magnetic fields is complex, the situation for real ocean currents allows for considerable simplifications. As the vertical velocity is small compared to the horizontal components, the cross product of $\vec{U}$ and $\vec{B}$ produces only horizontal fields depending on $u$, $v$ and $B_z$

Thus the evaluation of eq. (52) yields for the horizontal component

$$\vec{\nabla}_h\varphi = (\vec{U}_h \times \vec{e}_z B_z) - \frac{1}{C}\vec{i} \qquad (2.6)$$

where h stands for horizontal and $\vec{e}_z$ is the unit vector in z direction.

The potential gradient can be measured by two electrodes spearated by a distance L as in Fig. 2.11 which shows the situation of a current flowing through a strait.

The two electrodes can also be towed behind a ship. This arrangement is known as the GEK, the geomagnetic electro-kinetograph. Assuming the electrodes to be perfectly aligned on the ship's course and at equal depths the circuit does not cut field lines in the direction of the moving ship. This provides an elegant method to measure currents perpendicular to the ship's course if the leeway of the towing vessel can be neglected or measured by other means.

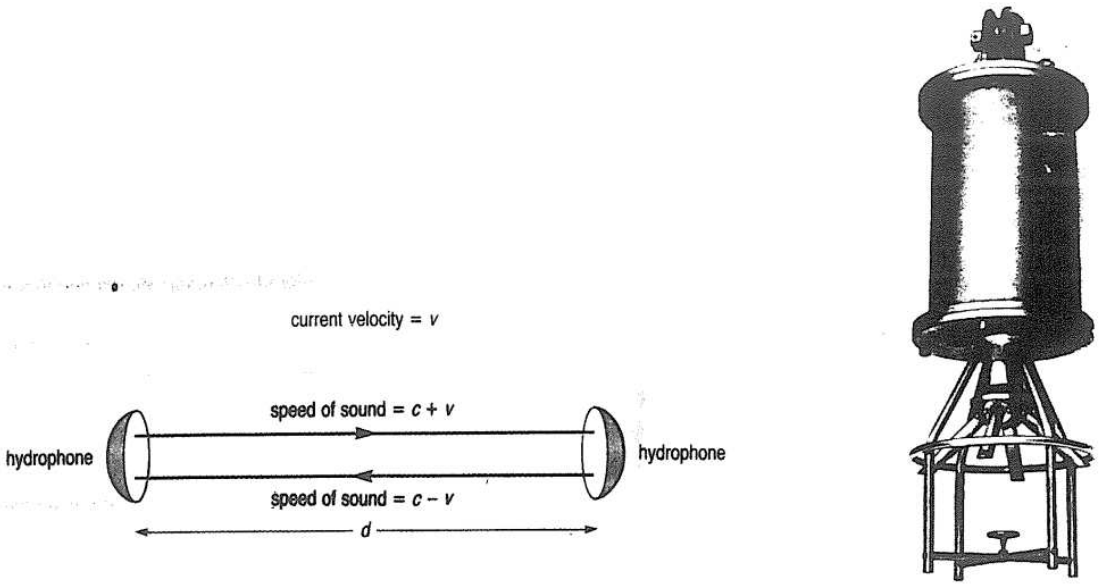


Fig 2.13 Principle of a travel time current meter and an example of a commercially available instrument based on this principle.

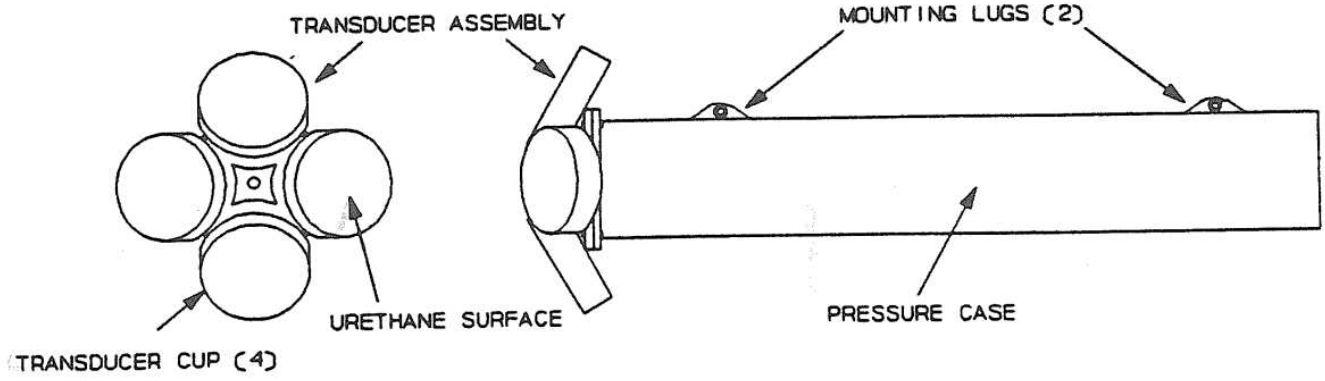


Fig 2.14a Acoustic Doppler current profiler (ADCP).

The fixed electrodes measure directly the motional electromagnetic force minus the voltage drop due to the resistance of the conducting water and sea floor.

One of the severe problems connected with GEK measurements concerns the electrodes. With an ocean current of 100 cm $s^{-1}$ and electrode distance of 20 m, a typical signal ranges is in the order of 1 mV. The offset potential between electrodes in the same sea water can sometimes reach the same level.

It is obvious from the small field strength of the natural magnetic field that it cannot be used in connection with small sensors on the centimeter scale. Artificial magnetic fields have to be applied in this case and ac fields are used to avoid difficulties with the electrodes. Most of these current meters have a vertical magnetic axis to measure horizontal current components.

A second goal in constructing such sensors concerns the interference of the flow with the rigid sensor body. It is necessary to have the electrodes outside the boundary layer of the housing. Only if the pattern of fluid flow around the sensor is similar for all velocities, the output will be a linear function of speed and the electrical voltage induced will change sign with the velocity vector.

No moving parts, two-component measurement and fast response characteristics are the most attractive features of electromagnetic current meters which are not only used in oceanography. In this field they have found first applications in shallow water, in connection with the measurement of orbital velocities and with turbulence studies near the sea floor (Fig. 2.12).

The definition of velocity suggests measurement of travel times at a constant measuring distance, which provides an Eulerain sensor when the distance is sufficiently small. Imagine a heating coil that warms up a small volume of water periodically. It flows downstream and is sensed by a thermistor, at a fixed distance from the coil. As soon as the thermistor has registered, a new pulse is sent to heat the coil. The time interval is measured.

In oceanography travel times are measured between mutually exciting and receiving sound sources A and B facing each other at distance L. The difference between the frequencies f registered is a measure for the (Doppler shifting) water velocity v along the path between the two sources/receivers

$$f_{AB} - f_{BA} = \frac{v}{L}$$

The basic problem is the detection of very small travel time differences of O ($10^{-10}$s) and the probe has to combine mechanical strength with minimum interference with the flow field, especially the wake generated by an upstream probe.

A nowadays quite commonly used type of instruments measures the water velocity by reflecting a sound or light pulse on small particles like phytoplankton cells that are assumed to move on average with the ambient flow. Application is made of the Doppler effect, the frequency change induced by a moving wave source. Restricting ourselves to acoustic Doppler current profilers (ADCP), the instrument transmits a sound pulse in a beam of finite width and then listens to reflecting bugs, that act as moving sound sources, provided they are at least

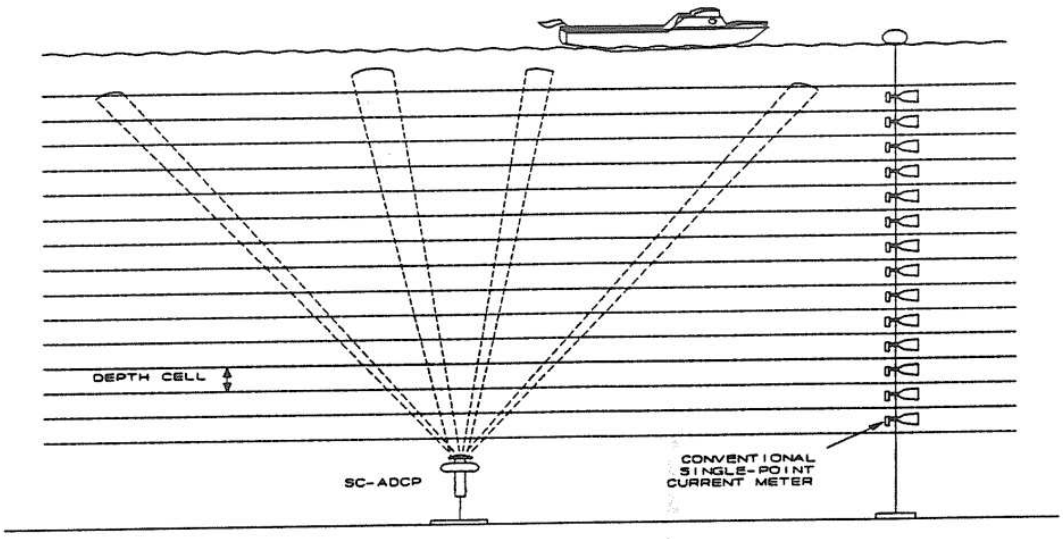


Fig 2.14b Advantage of ADCP measurements.

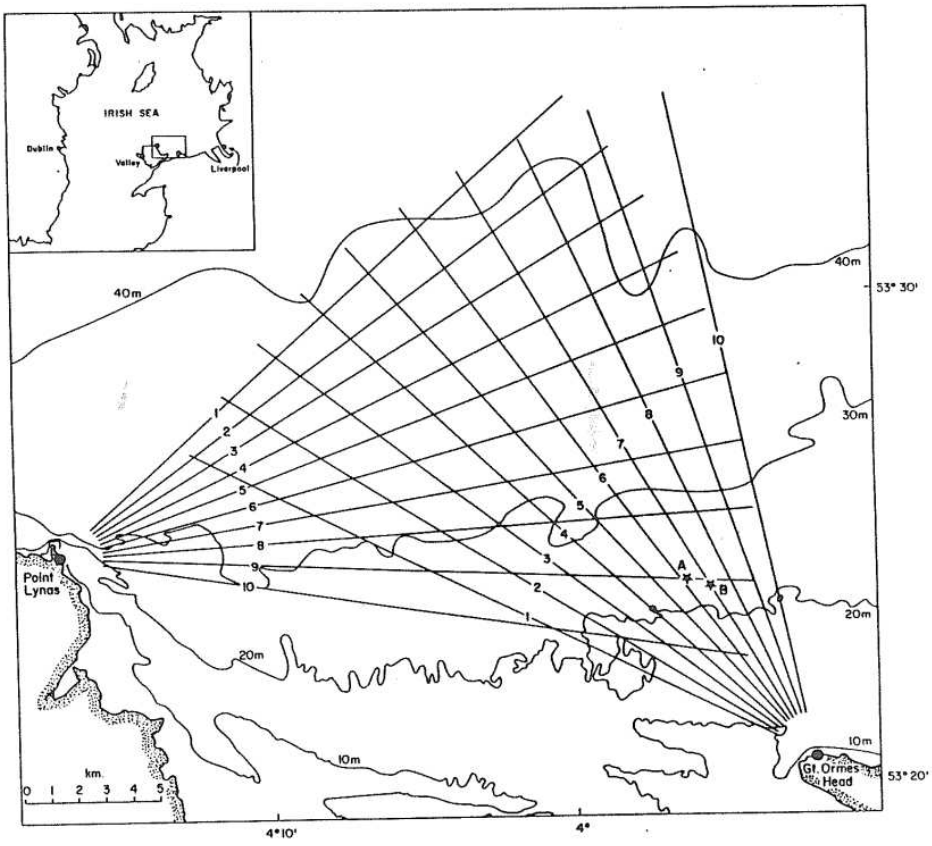


Fig 2.15 HF Radar beams over the Irish Sea.

greater than half the wavelength of the sound emitted. The instrument then measures, per control volume, the Doppler shifted frequency

$$f_D = \frac{2\,v\,f_e}{c} \qquad (2.7)$$

where $f_e$ is the emit frequency, $c \approx 1500$ m/s the speed of sound and v the water velocity in the direction of the beam. Multiple beams slanted with respect to the instruments' axis, provide estimates of two or all three velocity components.

The great advantage of this method is that the instrument does not obstruct the flow. Furthermore, sufficiently powered sound sources and suitable range gating provide current velocity estimates at multiple layers at distances well away (10 - 100's of m) from the instrument. Disadvantages like large noise values are caused by the highly variable size and amount of scatterers in the ocean. It is diffficult to use these instruments in clear waters and near strong reflecting bodies like the ocean's surface or bottom. An example of such instrument is shown in Fig. 2.14.

Finally, shore-based HF (high frequency) radar is used to map out surface currents for quite large areas (Fig. 2.15). The emitted radio waves with wave length $\lambda_R$ are reflected on short surface waves of which those of $\lambda_w = \frac{1}{2}\lambda_R$ show spectral "Bragg" peaks that are offset by Doppler shifting due to large scale currents.

## 2.3 Indirect methods

Indirect methods involve measuring some property other than the motion of the water, from which the motion can be deduced. Two types of property may be considered suitable: those responsible for causing the currents and those that result from the currents. In practice these two categories are often indistinguishable, becuase currents affect the distribution of the properties, such as density, which in turn determine the pattern of currents. In the oceans changes are constantly taking place and readjustments are occurring both in the current field and in the density field. Here we generally assume that a balance exists, however, and that the current field can be deduced if the field related to it can be specified.

If we assume a geostrophic balance (Chapter 1) and if we are observing in a homogeneous sea, we could use data from pressure gauges some distance apart. In stratified water, when lines of constant density do not coincide with levels of constant pressure, vertical profiles of density, measured by lowering a CTD probe at stations some distance apart, allow the computation of estimates of the geostrophic current induced by horizontal density differences. The equation of state is used to transfer conductivity C, temperature T and pressure ($\approx$ depth D) to density. Variations in the height of the sea surface, which are related to variations in pressure, are measured nowadays by satellites. This altimetry is a promising tool for the study of the large ocean circulation as well as small scale features like Gulf Stream eddies.

The principle of continuity can, for an incompressible fluid like water, be used for estimates of flow variation as a function of changing dimensions in comparatively restricted bodies of water. The flux $F_u$ through a cross sectional area A should be constant

$$F_u = Au \qquad \textbf{(2.9)}$$

where u is the flow component. In addition, the distribution of salt may be used by means of investigation of the salt fluxes to compute the average advective current.

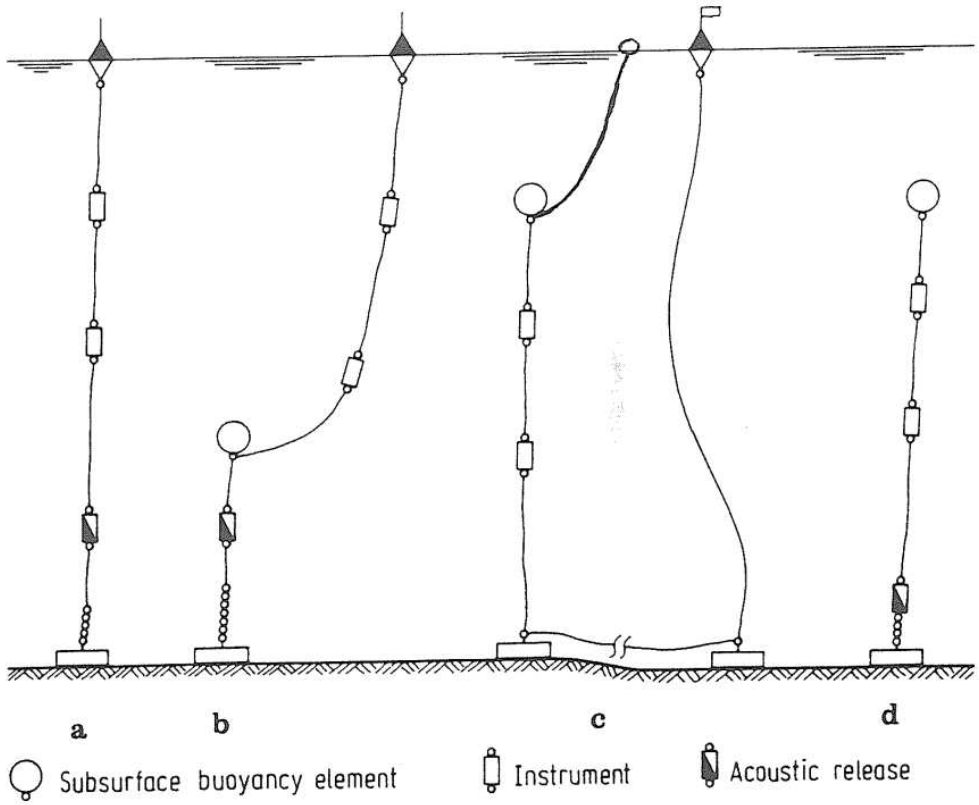


Fig 3.1 Different types of moorings. Surface moorings: taut wire mooring (a), slack wire mooring (b). Subsurface moorings: ground-line mooring (c), single point mooring.

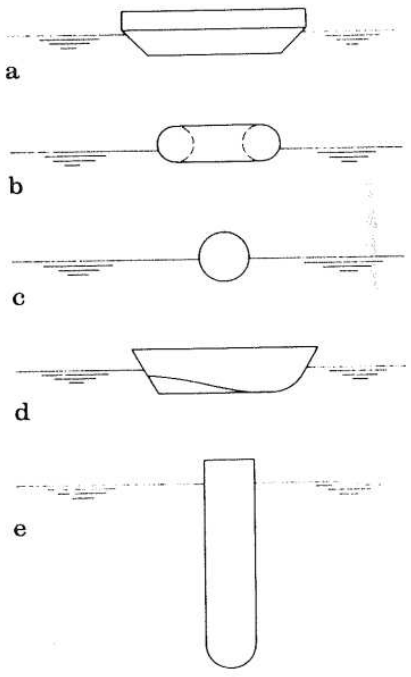


Fig 3.2 Generic buoy forms. Disc (a), Torus (b), Sphere (c), Boat (d), Spar (e).

# 3. Instrument moorings

Instrument moorings are used for obtaining time series at a fixed position of data. Multiple moorings in a sea area are used to obtain synoptic data of the flow field in that area. Several mooring configurations are sketched in Fig. 3.1. Regardless whether a buoy is seen at the surface or not, the classification is based on the location of the main buoyancy element for upholding the instrumentation.

Basically a mooring consists of an anchor or weight at the bottom, connected to a line or chain of sufficient strength to which the instruments are attached by schackles and swivels. Floats that must be able to withstand large environmental pressure when used at great depths (10 m $\alpha$ 1 bar) are used to uphold the line of instruments. All materials must be able to endure long exposure to corrosion, the effects of strong currents, the impact of life at sea in terms of growth on the instrumentation or agressive fish that may bite through nylon mooring lines. Activities of man may pose a problem, especially in shallow seas, as moorings may be hit by vessels or entirely wiped out by fishing nets.

## 3.1 Types of mooring

Surface moorings are subdivided into taut wire (Fig. 3.1a) and slack wire (Fig. 3.1b) moorings depending on whether the length of the mooring line is approximately equal or larger than the water depth.

All surface moorings have the disadvantage of high loading on all mooring components and instruments. This is particularly true for taut wire moorings, but these have the advantage of small buoy watch circles and small horizontal excursions of instruments under varying current conditions.

The dynamical loading of a surface mooring depends on the type of buoy used. Surface-following buoys (types b to d in Fig. 3.2) provide large buoyancy to support long deep-sea moorings but they move heavily under the action of waves thus inducing severe stresses to the system and "noise" to the time series to be measrued. With spar buoys wave action on the mooring can be suppressed, but the buoyancy safety margin can be a problem in areas with strong currents. Large spar buoys are necessary for measurements near the surface, both in air and in water. This type of mooring is generally not suitable for measuring currents at sea, except in areas where the wave action is expected to be low.

Current measurements in the deep ocean are usually made in a single point subsurface mooring (Fig. 3.1d). Sufficient surplus of (positive) buoyancy at the float is required to keep the mooring line taut. The mooring is deployed by letting the float drift away from the ship, attach instrumentation and finally release the weight. Upon recovery an acoustic release is activated by the ship's echosounder or via separate hydrophones hanging over the side of the ship. The anchor and weight are left at the bottom. An acoustic release responds to two different acoustic frequencies before release, to avoid mooring loss by dolphins, talking to the instrument.

The disadvantage of such mooring type is that loss or leakage of the main buoyancy package will result in entire loss of instrumentation.

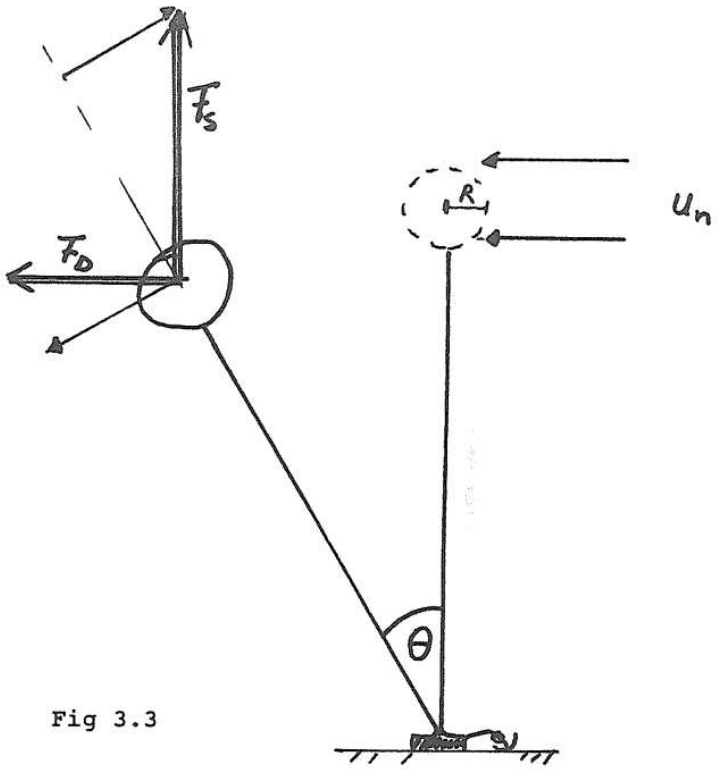


Fig 3.3

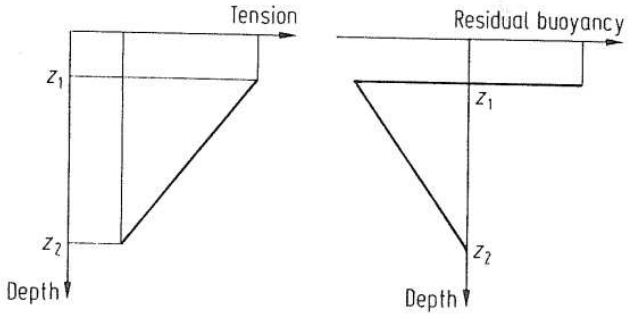


Fig 3.4 Tension in the mooring line and residual buoyancy as a function of depth for a primitive mooring consisting of an anchor at z2 and a single buoyancy element at z1.

In shallow seas the ground-line mooring is the most common type (Fig. 3.1c). No expensive acoustic releases are needed. The surface buoy is used as a mooring guard, to warn other vessels, but also provides a second chance of recovery once the instruments' pick up line is broken. A third chance of recovery, when the subsurface buoyancy and the guard buoy are lost or leaking, is provided by the ground line of typical length of 100 m, that may be caught by a dredge.

Deployment of such mooring requires some skill. Firstly the weight of the instrument line is held over the side. Instruments are successively atttached while the weight and the connected ground line are lowered. The problem is to avoid entanglement of the ground line and the instruments as the two lines cannot be separated over a wide distance (usually the width of the ship). After the release of the surface float of the instrument line the ship drifts away while slowly the ground line is released before the anchor and surface buoy are lowered.

For both types of moorings the subsurface float should be well below the sea surface (10-15 m) to avoid large exposure to orbital surface wave motion. Hence, these moorings cannot be used in very shallow waters.

## 3.2 Some aspects of mooring design

Mooring design starts with knowledge of the materials that will be used. One should know the breaking strength, both under continuous static tension and under impulsive action, of the line, chains and shackles. The buoyancy or weight in water of all of the materials and instruments have to be known. For a spherical float the net positive buoyancy force is

$$\begin{aligned} F_b &= (\rho_w - \rho_m)\, g\, V \\ &\approx \rho_w g\, {}^4/_3\, \pi\, R^3 \end{aligned} \qquad \textbf{(3.1)}$$

where R is the radius of the sphere, V its volume and $\rho_m$ its density (usually roughly equal to the density of air: $\rho_a \approx 1$ kg/m$^3$) and $\rho_w \approx 1025$ kg/m$^3$ the density of water. The acceleration of gravity is denoted by g.

Under the action of a current the mooring line will be deflected from the vertical. If one assumes that tension in the wire and the buoyancy is not much changed by the current, equilibrium with drag forces is reached when the mooring line assumes a respective shape.

The positive buoyancy in the mooring should be chosen such that the net buoyancy cancels out (part of) the deflective effects by drag forces under the consideration of the line strength. If we assume for a moment that most of the drag force is induced at the subsurface float only, which is generally the case in shallow sea moorings, the relevant balance of forces in equilibrium state reads

$$F_S \sin\theta = -\tfrac{1}{2}\, \rho_w\, C_D\, A\, |\vec{U}|\, u_n \cos\theta \qquad \textbf{(3.2)}$$

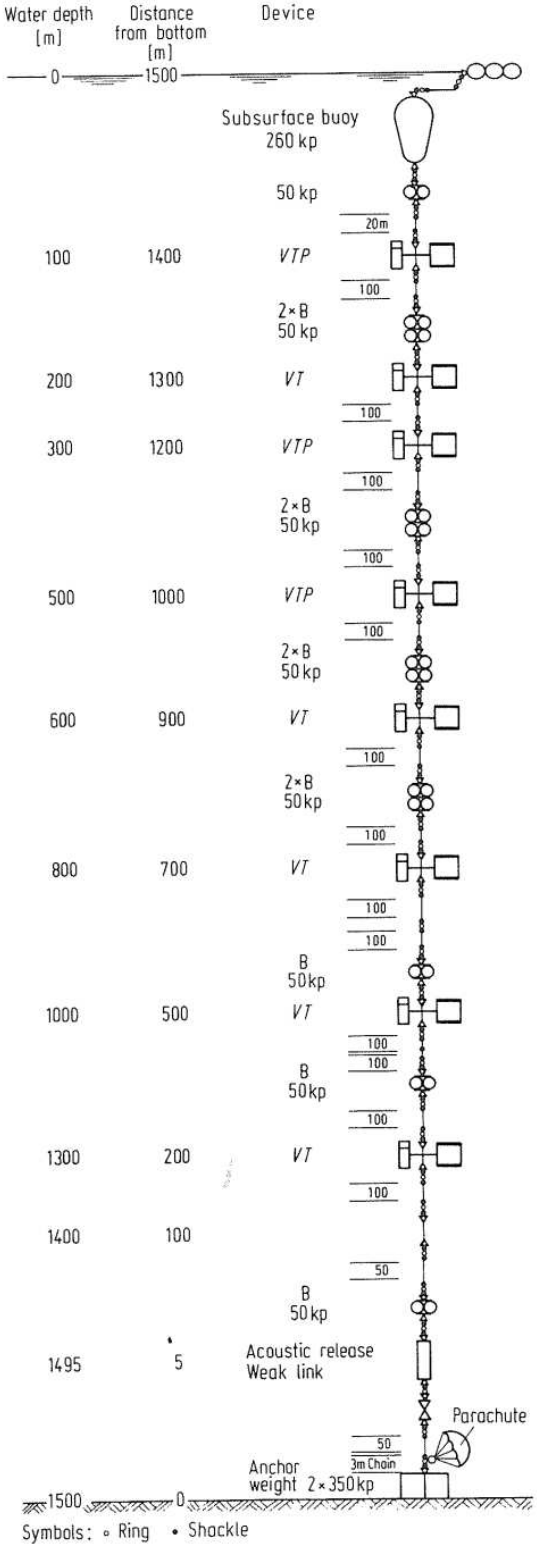


**Fig 3.5 A deep-ocean mooring.**

where $F_S$ is the net buoyancy force and where $\theta$ is the deflection angle of the mooring line, $u_n$ is the normal velocity component, A is the area exposed normal to the direction of the current and $C_D$ is the drag coefficient (Fig. 3.3).

Then, at the float, the mooring is lowered vertically over a distance

$$h = L\,(1 - \cos\theta) \qquad \textbf{(3.3)}$$

where L is the length of the line from the weight to the float. In shallow seas h should not exceed values of O(1 m).

The tension force $F_Z$ in the line should balance the sum of the tangential components of the drag force and the buoyancy force:

$$F_z = F_S \cos\theta + \tfrac{1}{2}\rho C_D A u^2_n \sin^2\theta \qquad \textbf{(3.4)}$$

assuming that the tension is reduced to zero at the anchor.

In deep oceans long mooring lines are not uncommon and multiple buoyancy packages are used to keep the mooring upright (Fig. 3.5) The total mooring may be exposed in currents of different magnitude and direction with height. Computer programs are used to perform calculations on the mooring line shape. To obtain this shape, the total mooring line is subdivided into a number of segments and drag and buoyancy forces are computed per segment that are thought of a rigid cilinder connected via universal joints.

The following definitions (see Fig. 3.6) are necessary for practical computations and are taken from Krause (1986). A vertical line through the anchor and the deflected mooring line (direction $\varphi$ with respect to North) defines a plane which is referred to as the reference plane. A current vector pointing in a direction ($\gamma$-$\varphi$) with respect to this reference plane causes drag forces *F* which tend to bend and to rotate the mooring line into the current direction *y* with respect to North.

The velocity component relevant to the calculations of the drag forces are

$V_F$: velocity component in direction of the reference plane, and

$V_N$: velocity component perpendicular to the reference plane,

$$V_F = V.\cos(\gamma-\varphi)$$
$$V_N = V.\sin(\gamma-\varphi)$$

*V* is the magnitude of velocity vector

With respect to a point *P* on the mooring line we have

$V_T$: velocity component of $V_F$ along the mooring, and

$V_{TN}$: velocity component of $V_V$ perpendicular to the mooring.

If $\theta$ is the angle of deflection of the mooring line from the vertical we have

$$V_T = V.\cos(\gamma-\varphi)\sin\theta\,,$$
$$V_{TN} = V.\cos(\gamma-\varphi)\cos\theta$$

The respective drag forces are

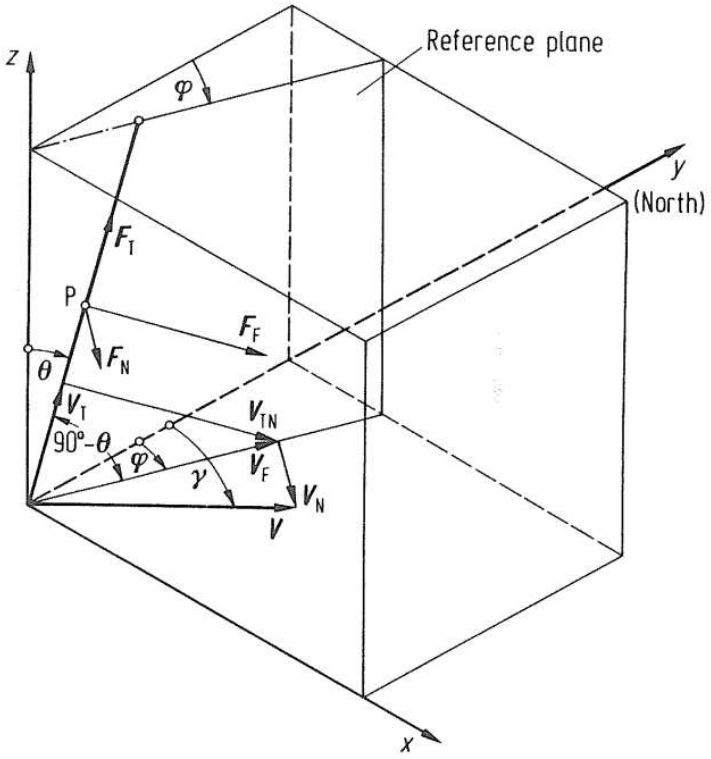


Fig 3.6 Definition sketch of forces on a mooring segment with centre P submersed in a flow with velocity V.

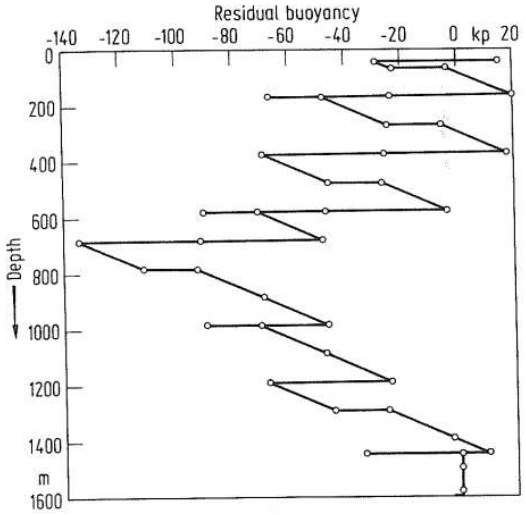


Fig 3.7 Distribution of the residual buoyancy with depth, as computed for the mooring in Fig 3.5. The large contribution of the subsurface buoy (2700 N) is not indicated.

$F_T$: component tangential to the mooring line in the reference plane,
$F_F$: component perpendicular to the mooring line within the reference plane,
$F_N$: component perpendicular to the reference plane. This component causes rotation of the mooring line.

Using the quadratic law for the drag force one obtains

$$F_T = \tfrac{1}{2}\varphi.C_{DT}.A_L.l. \mid V_T \mid V_T,$$
$$F_F = \tfrac{1}{2}\varphi.C_{DN}.A_L.l. \mid V_F \mid V_{TN}$$
$$F_N = \tfrac{1}{2}\varphi.C_{DN}.A_L.l. \mid V_N \mid V_N$$

where $C_{DT}$ is the drag coefficient along, and $C_{DN}$ the respective coefficient perpendicular to the mooring line. $A_L$ is the area per unit length of a mooring segment and $l$ is the length of a segment, $\varphi$ denotes density.

Finally we have to consider buoyancy and weight.
$F_S$: sum of buoyancy and weight.
It has the normal and tangential components

$$F_{SN} = F_S.\sin\theta,$$
$$F_{ST} = F_S.\cos\theta$$

In the equilibrium state the vectorial sum of the forces must be zero. This means in components

$$F_{SN} + F_F = F_{zn-1}.\sin(\theta_n - \theta_{n-1}),$$
$$F_{ST} + F_T = F_{zn} - F_{zn-1}.\cos(\theta_n - \theta_{n-1})$$
$$F_N = F_{zn-1}.\sin\theta_{n-1}.\sin(\varphi_n - \varphi_{n-1})$$
$$F_{zn}\sin\theta_n = F_{zn-1}.\sin\theta_{n-1}.\cos(\varphi_n - \varphi_{n-1}),$$

where $F_{zn}$ is the force due to the tension in the n-th segment of the mooring line. These equations can be used for an iteration calculation of the equilibrium state. The force at the topmost segment is used as the starting value. If $\theta'$ and $\varphi'$ denote the vertical and azimuth angles, respectively, resulting from the previous iteration step, equilibrium is reached when

$$\Delta\theta = \theta_n - \theta',$$
$$\Delta\varphi = \varphi_{n-1} - \varphi',$$

are smaller than given values. Replacing $\theta_n$, $\varphi_n$ by $\theta'$, $\varphi'$ the final equations are

$$F_{zn} = F_{zn-1}.\cos(\theta' - \theta'_{n-1}) + F_{ST} + F_T$$

$$\theta_n = \arctan\frac{[F_{SN} + F_F - F_{zn-1}.\sin(\theta' - \theta'_{n-1})]}{F_{zn}} + \theta'$$

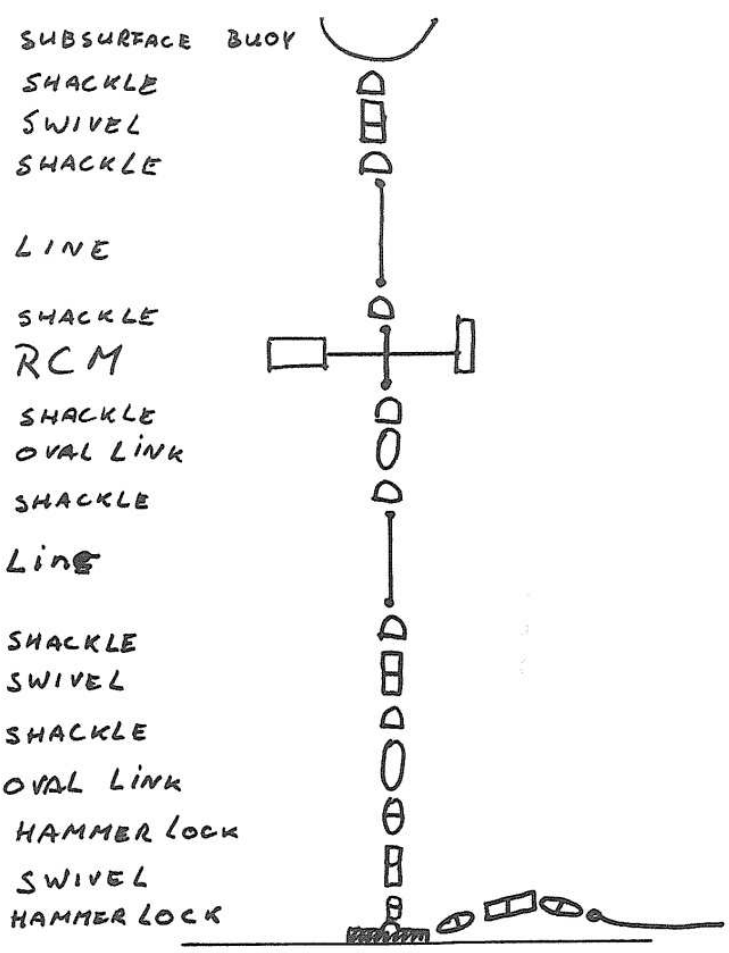


Fig 3.8 A sequence of mooring materials.

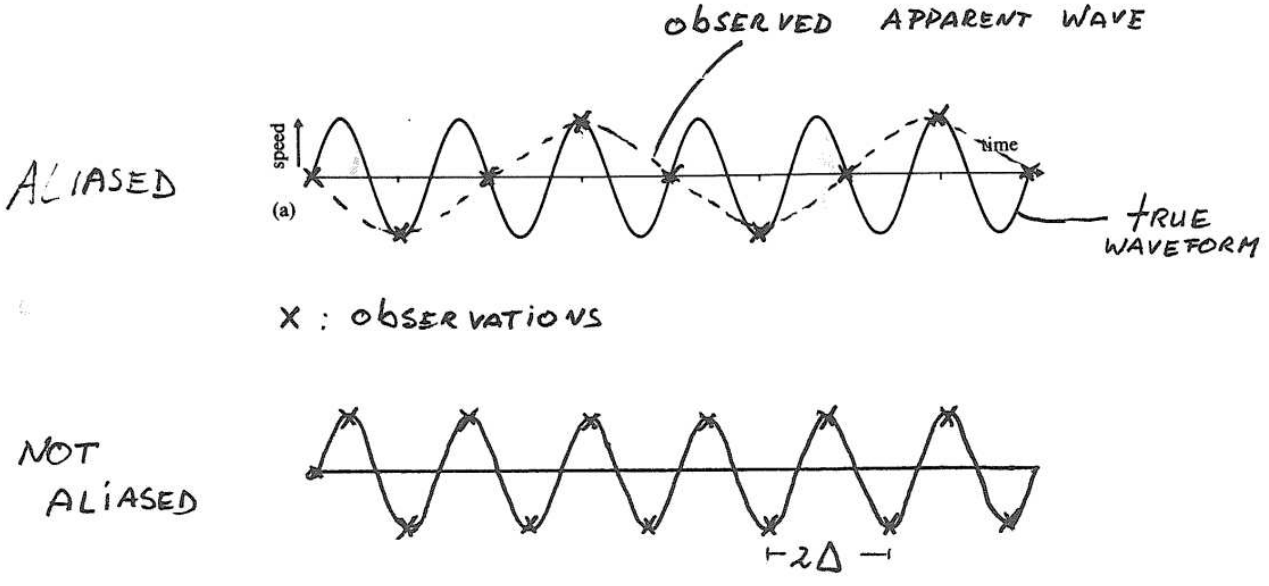


Fig 3.9 The effect of aliasing.

$$\varphi_n = \arctan\left[\frac{F_N - F_{zn-1}.\sin\theta_{n-1}.\sin(\varphi' - \varphi'_{n-1})}{F_{zn}.\sin\theta_n}\right] + \varphi'$$

A practical application of such calculations is given in Fig. 3.7. As strong surface currents have the greatest effect on mooring displacement, a pressure recorder should always be included near the uppermost current meter. Additional attention must be given to the elasticity of mooring lines and technical details of mooring components such as swivels to avoid unwanted twisting of the line by drag Jones acting perpendicular to it.

Strong currents may have other effects on current measurments in a mooring like depicted in Fig. 3.5. the effects have been reported of mooring vibrations, induced by the action of currents on the subsurface floats, on currents measurements by paddlewheel rotors-equipped instruments.

## 3.3 Mooring materials

A large variety of materials is used in ocean moorings. Details on breaking strength and resistance against adverse corrosive impact can not be given here. They depend on the specific sort of material used. A list of characteristics of some materials used at Bedford Institute of Oceanography, Canada, is given in Table 3.1 The static mooring tension should never exceed 33% of the breaking strength of the materials.

Lines made of kevlar are often used for deep ocean moorings. This material has good weight versus strength characteristics, but is expensive. They are subject to fish bite and are not used at depth greater than 2000 m. In shallow seas moorings with nylon or coated steel lines are generally used. Nylon lines are thicker than kevlar of the same strength, but are slightly positively buoyant. This has disadvantages when such lines are used as a ground line; the floating line might entangle with the instruments. Another disadvantage of nylon lines is their fast biological fouling, and hence variable buoyancy. Steel lines may be thinner but are heavier than nylon. Because of their stiffness they should be handled with care to avoid kinking. Their major disadvantage is their sensitiveness to corrosion. They should be well coated.

Sub-surface floats should be able to withstand the environmental pressure and corrosive effects that lead to leakage and loss of buoyancy. Spheres withstand pressure best and have low drag coefficients and glass balls are commonly used. When other materials like polyester are used, the spheres are usually filled with waterresistant foams.

All links between instrumentation and the mooring line should be made of stainless steel for moorings that will be deployed for periods longer than a week, say. Oval links are used to hold the mooring line while de(at)taching instruments during recovery (deployment). Shackles should be well securable and easy to handle during the overboard operations. Swivels are used on one or either end of not freely rotatable parts, like floats and anchor wieghts. A typical sequence of materials used for a shallow water mooring is presented in Fig. 3.8.

## 3.4 Sampling times

Ocean currents appear at a large variety of time scales, in fact linked together in a more or less continuous spectrum. A current meter however, does not measure currents continuously or ad infinitum, but at discrete intervals $\Delta$ regularly spaced in time during a finite period T, which is limited by battery life and data storage capacity. The sampling interval and the record length each impose false current observations one needs to avoid depending on the currents one wants to observe.

Recording the current magnitude and direction once every $\Delta$ = 10 min say, does not simply mean that we do not observe currents that are periodic at $T_p < \Delta$ . Energy that is contained in such currents shows up at lower frequencies, a process called aliasing. Discrete sampling at frequencies $\sigma = 1/\Delta$ in fact represents viewing through a slit data window opening at regular intervals. The highest frequency possible to detect correctly is the Nyquist frequency $\sigma_N=1/2\Delta$ (Fig. 3.9). All higher frequencies are incorrectly sampled and appear as lower frequency motion. In the spectral domain this may be represented by backfolding the (unknown) high frequency spectrum at $\sigma_N$, with energy at $\sigma = 1/\Delta$ (+ $2/\Delta$...) adding to energy contained at $\sigma = 1/T$.

Fortunately, the oceanic spectrum is red (most energy is contained at low frequencies) and for typical current observations of tides and lower frequency motions aliasing is not a problem, provided the Nyquist frequency is well away ($\sigma_N > 10\ \sigma_0$, say, where $\sigma_0$ is the frequency of interest). A noteworthy dissonant may be the influence of surface waves, when currents are measured close to the ocean's surface.

We already mentioned that all motions at frequencies $\sigma < 1/T$ will appear lumped together in a finite length data record. They are not resolved by such time series. Within a record of duration sufficient to resolve a certain group of periodic motions, unresolved motions may also occur when their frequencies are not well separated. If one wants to distinguish motions oscillating at frequencies $\sigma_1$ and $\sigma_2$, for example the Moon's and Sun's semidiurnal tides, the minimum record length is given by $T_{min} = |\sigma_1-\sigma_2|$ , known as the Van Abbe criterium (Rayleigh proposed a slightly less strict criterium). For the semidiurnal tides above this means $T_{min}$ = 14.7 days, the fortnightly beat of springs and neaps.

The reason behind this has do to with the Fourier transform of a finite time series (Chapter 4). We effectively view the infinite time series through a window of width T. This results in a broadening of spectral peaks over a width of about 2/T in the frequency domain, which will overlap indistinguishable when they come within a frequency reach of about 1/T with each other. It should be noted that it is advantageous to choose the record length such that it is an exact multiple of $T_{min}$. This ensures there is no leakage from one sine wave to the other. For a proper investigation of non-deterministic motions at known frequencies, a data record should be even longer for sufficient statistical significance.

CURRENT METER FORM

Cruise :
R. Vessel :

Position of mooring North : West:
Local waterdepth :

Current meter type : number:
Sensors installed :
Sampling interval (s):

Position in the mooring
Depth below the surface (m):
Depth above the bottom (m):

First reading date (ddmmyyyy): time (UTC):
Mooring deployed date (ddmmyyyy): time (UTC):

---

Start retrieval date (ddmmyyyy): time (UTC):
Stop sampling date (ddmmyyyy): time (UTC):
Number of data expected: sampled :

REMARKS

Fig 3.10

## 3.5 Procedure for experiment set-up

Once the site and the observational goal have been chosen, current meters can be prepared and set-up. For every deployment a checklist for mechanical inconsistencies and performance inspection of the meters should be used. The instruments' logbook should be checked for performed repairs. Sensor calibration sheets, especially of the compass and additional sensors, should accompany the instrument. Calibrations should be of recent date, preferably shortly before deployment. New batteries and, if necessary, new tapes should be installed.

Every instrument on each mooring is accompanied by a log sheet as in Fig. 3.10. Time and date of first reading as well as location of the instrument on the mooring are carefully noted. Sampling intervals are chosen as a function of battery life and data storage capacity as a function of intended deployment duration.

Preparation of the mooring starts with a choice of materials. Once these are known together with the number and specifications of the instruments to be moored, vital characteristics of a hypothetical mooring can be computed. Of interest are the expected tension in the mooring line and the distribution of buoyancy and expected deflection from the vertical. Such computations may result in alterations in the choice of materials. Once the repititive steps of material choice and design computations have been satisfactorily completed, a detailed mooring design is drawn.

The deployment of a mooring in national and international waters requires notification of several authorities. Usually the navy, but certainly seamen and agencies responsible for navigation in sea areas should be notified well in advance. This allows for implementation of buoys in sea charts.

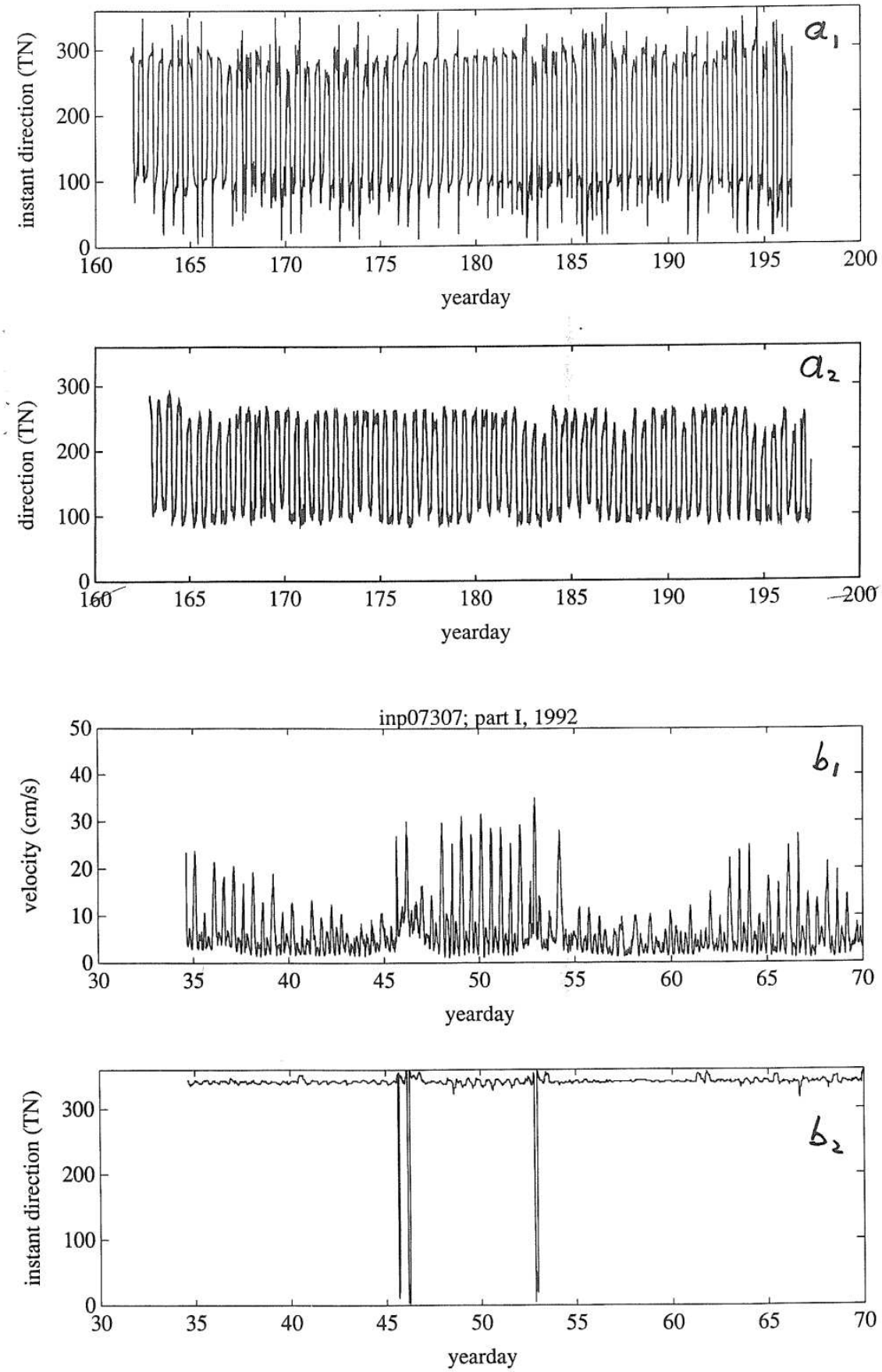


Fig 4.1 Examples of current meter records. Correct direction data (a1) can be compared with imperfect direction data (a2) measured by two different current meters in the same mooring during the same period of time. Is a ground-line problem detected in (b)?

# 4. Data analysis

The analysis of a time series of current meter data, or any other data record, consists of two parts; the raw data analysis and the time series analysis. Every instrument has its limitations and hence adds unwanted "noise" to a data record. It may at times store incorrect data, that show up as "spikes" in the record. The finite length of the record and the discrete sampling interval also add, together with adverse environmental conditions, unwanted signals to the record. During the raw data analysis the observer should be aware of these impacts and accordingly try to clean up the data set. In doing so, he or she may want to use sophisticated tools that are also used for the time series analysis, when the nature of the observed currents is explained.

## 4.1 Raw data analysis

All analyses start with a gathering of information on the expected currents for the area of investigation. Knowledge on the (relative) importance of tidal, wind driven and long-term currents should preferably be available. Secondly, the instruments' log sheet should be considered for remarks on the visual inspection after retrieval of the mooring.

The first check on the validity of the data exists of the computation of the expected number of data $N = T/\Delta$, where T is the period of measurements and $\Delta$ is the sampling interval. After the data have been read the length of the record n should not differ from N ($|N - n| > 1$).

If this is not true, a digital check on the data read should focus on missing syncs. The data gaps may be filled by interpolating between neighbouring data points when the gaps are small. In a highly variable current regime large gaps are difficult to interpolate.

The first tool in the analysis is the plot of the time series of current magnitude and direction, as supplied by the instrument, and of the two current components they can compose. Such graphs enable us to look for "wild" observations or "outliers", which do not compare with the rest of the data. The treatment of outliers ("despyking") is a complex subject in which common-sense is more important than statistical theory. General threshold levels between neighbouring data points can not be given. Possible examples will be indicated below.

Despyking is performed visually and manually. Obvious erroneous measurements like the begin- and endpoints of the record, when the meter was not moored, need to be removed. Knowledge of the expected currents is helpful. For example when current magnitudes lower than 0.1 m $s^{-1}$ are expected, values of
1 m $s^{-1}$ , occurring suddenly, probably are erroneous. When detected as such, outliers are adjusted to their expected values under normal conditions via interpolation between neighbouring datapoints. A few spykes occur in almost any record. When a large number of data points (> 10% of n say) are denoted as outliers, the instrument should be tested for electronic faults.

An instrument definitely needs repair when the time series plots show a constant value of either the current magnitude or direction. Subtle errors may be detected when the time series do not entirely compare with expected values. In a

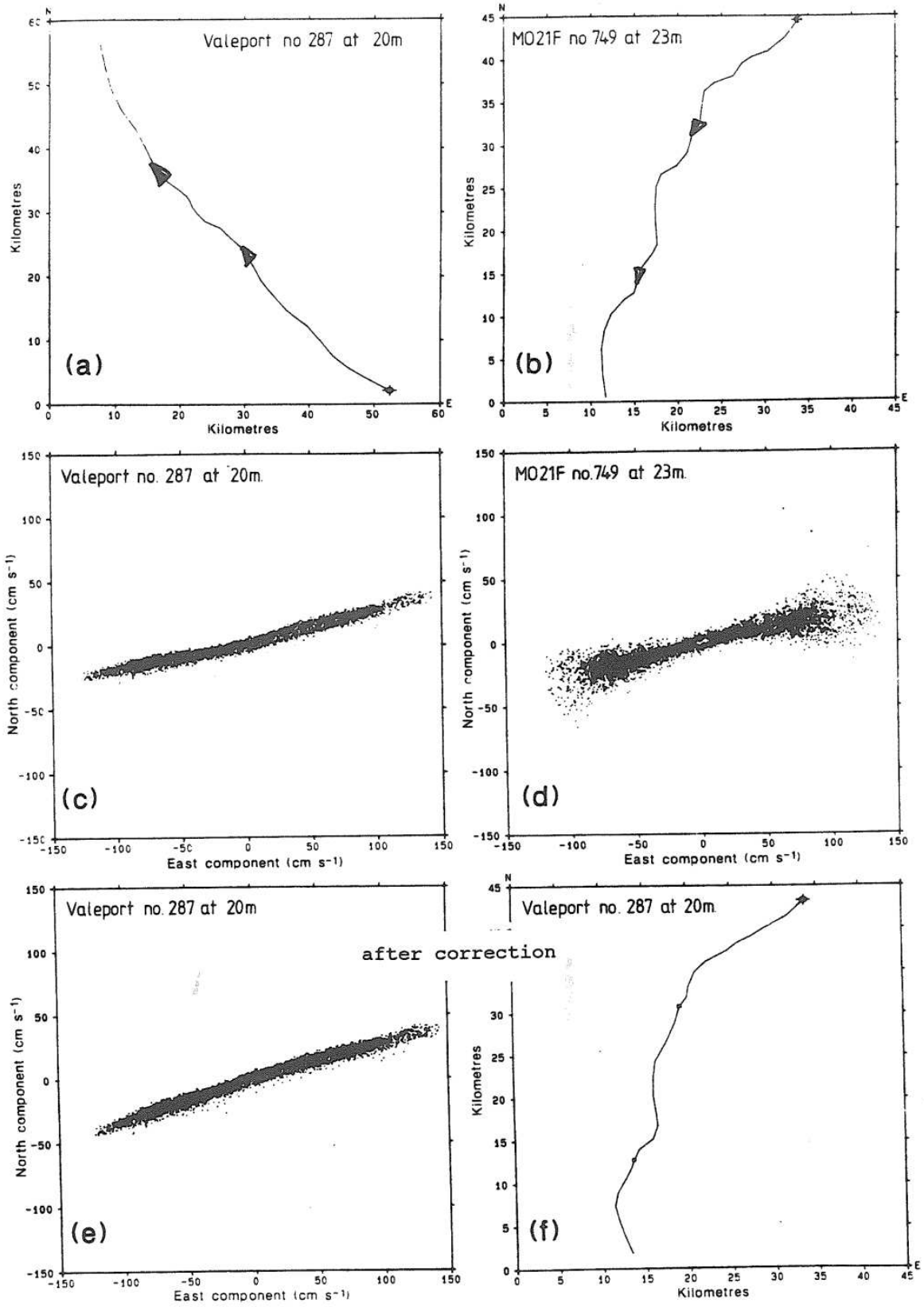


Fig 4.2 Progressive vector diagrams (a and b) of tidally filtered current data, measured by two different instruments in the same mooring, show a remarkable discrepancy.

tidal current regime for example, the direction should (once in a while) cover all of the [0° , 360°] domain, even when the principal axis of motion is directed East-West (Fig. 4.1a). A missing bit may be the cause of not-occurring values. If the record can not be repaired at the bit level, it should entirely be discarded. The same holds when a record shows an asymmetric behaviour with the direction of the tidal current. This may (but need not!) point at a stiff gimbal or an entanglement of the instrument with a ground line (Fig. 4.1b). If this is found, the record should not be analyzed further.

Under general use, current meters sample data that are well away (in frequency) from environmental and instrumental noise. When the records occur not smoothly varying, but have superimposed a large number of small spykes, referred to as "noise", the electronic circuit of the instrument needs repair. The record as such may be kept for further analysis, but the noise should be removed by suitable filtering (cf. section 4.2).

The mean current, obtained by averaging the velocity components over the full length of the records, is very sensitive to the proper measurement of the direction, especially when strong tidal currents are superimposed. Misfits between the observed mean current and its expected magnitude and direction should point at such error (Fig. 4.2). Similarly, knowledge of the tidal current regime from previous measurements or numerical models may be used to check the validity of the data by computing the tidal amplitudes and phases for the current components via harmonic analysis (section 4.2). Then, the possibility of measured internal tidal currents should be kept in mind before invalidating the records.

The validity check of data is greatly enhanced when two or more current meters, preferably of different make are located close together in the same current regime. Scatterplots of current magnitude versus current magnitude (Fig. 4.3), and similarly for direction u and v may highlight errors.

The outcome of the raw data analysis should be noted on the instruments' log sheet. They may be used for the history of performance of the instrument and possible deteroriation with time of one or more components may be detected before new deployment. the cleaned data set is submitted to further analysis.

## 4.2 Time series analysis

The intended analysis of the data can be separated in three parts, time domain analysis, spectral analysis and comparison with (flow regime) models. Here we describe (parts of) the first two only. The comparison with models, leading to model building from the data or validation of existing models with the data, may be the ultimate goal in ocean research, by finding a (dynamic) explanation of the observed currents. It is beyond the scope of this workshop however, as it depends too heavily on the region in where the instruments have been moored.

A typical ocean current meter record consists of two types of signals, deterministic and random signals. They describe processes of which (some) properties are known in advance, such as tidal signals, and processes such as turbulence that are (partly) described by a set of random variables and their probability distribution, respectively. Their analysis is quite different. Some mathematical function of time appears the major tool in the analysis of the

Fig 4.3

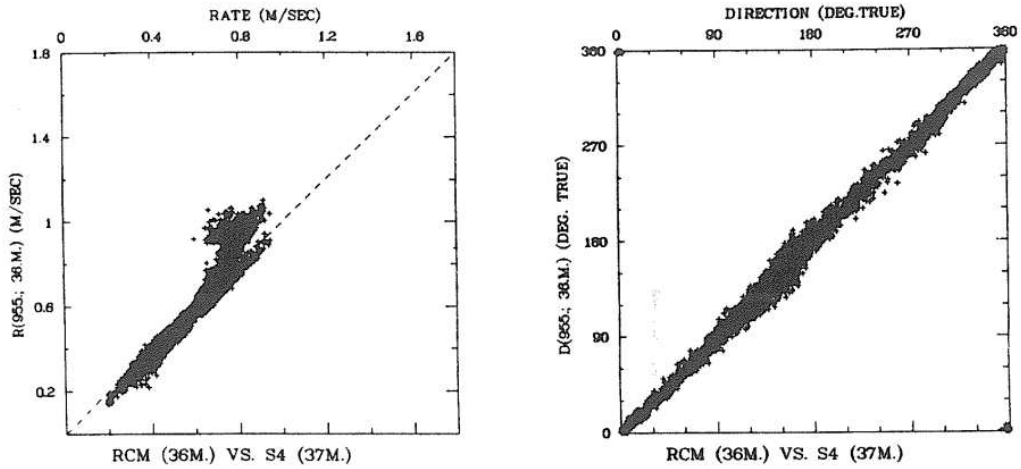


| Name of partial tide | Symbol | Speed (degrees per mean solar hour) | Period in solar hours |
|---|---|---|---|
| *Semi-diurnal components* | | | |
| Principal lunar | $M_2$ | 28.98410 | 12.42 |
| Principal solar | $S_2$ | 30.00000 | 12.00 |
| Larger lunar elliptic | $N_2$ | 28.43973 | 12.66 |
| Luni-solar semi-diurnal | $K_2$ | 30.08214 | 11.97 |
| Larger solar elliptic | $T_2$ | 29.95893 | 12.01 |
| Smaller lunar elliptic | $L_2$ | 29.52848 | 12.19 |
| Lunar elliptic second order | $2N_2$ | 27.89535 | 12.91 |
| Larger lunar evectional | $\nu_2$ | 28.51258 | 12.63 |
| Smaller lunar evectional | $\lambda_2$ | 29.45563 | 12.22 |
| Variational | $\mu_2$ | 27.96821 | 12.87 |
| *Diurnal components* | | | |
| Luni-solar diurnal | $K_1$ | 15.04107 | 23.93 |
| Principal lunar diurnal | $O_1$ | 13.94304 | 25.82 |
| Principal solar diurnal | $P_1$ | 14.95893 | 24.07 |
| Larger lunar elliptic | $Q_1$ | 13.39866 | 26.87 |
| Smaller lunar elliptic | $M_1$ | 14.49205 | 24.84 |
| Small lunar elliptic | $J_1$ | 15.58544 | 23.10 |
| *Long-period components* | | | |
| Lunar fortnightly | $M_f$ | 1.09803 | 327.86 |
| Lunar monthly | $M_m$ | 0.54437 | 661.30 |
| Solar semi-annual | $S_{sa}$ | 0.08214 | 2191.43 |

Table 4.1a Some principal tidal constituents

former, such as harmonic analysis, and statistical models are used in the analysis of stochastic processes.

The major objective of time domain analysis is to determine the behaviour of signals and their relation with other data with time. It is sensitive to bursting phenomena, large amplitude currents of limited duration occurring infrequently over the length of the records. Unremoved spykes will thus blurr such analysis. The average relative contribution of a signal per frequency band is studied in spectral analysis or frequency domain analysis, which is most sensitive to signals that are persistent throughout the period of observations.

### 4.2.1 Time domain analysis

The first step in time domain analysis is to use the plot of the observations against time. This will show features such as trend, seasonality, discontinuities. The mean and the trend, themselves interesting properties, are removed usually before further analysis.

If tidal signals are apparent, the horizontal current components are analysed via harmonic analysis, which makes use of known frequencies ($\sigma_i$) of the (harmonic) constituents. De facto the time series (u(t) for example) is compared with a time series $u_h(t)$ consisting of purely sinusoidal signals of amplitudes $a_i$ and $\varphi_i$

$$u_h(t) = a_o + \sum_{i=1}^{n} a_i \cos(\sigma_i t - \varphi_i)$$

The method to estimate the unknown ($a_i$ , $\varphi_i$ ) from a series u(t) is by the method of least squares. In this method the integral quadratic difference between the series

$$F(a_i, \varphi_i) = \int_0^T (u(t) - u_h(t))^2 \, dt$$

is minimized by zeroing all partial differentials

$$\frac{\delta F}{\delta a_0} = \ldots = \frac{\delta F}{\delta a_n} = \frac{\delta F}{\delta \varphi_0} = \ldots = \frac{\delta F}{\delta \varphi_n} = 0$$

The result will provide average estimates (over the length of the record) of amplitude and phase, with respect to the center of the record, for every component $\sigma_i$. For comparison with maps and previous data sets the phase has to be adjusted. The standard chosen is the time of passage through the meridian of Greenwich (UK). The corrections per component ($V_{oi} + u_i$), the astronomical argument, is deduced from the equilibrium tide and can be found in tables, such as table 4.1. This table gives ($V_{oi} + u_i$) for the beginning of the year and hence $\varphi_i$ have to be corrected accordingly first. Once $\varphi_i$ (beginning of the year) is known, the standardised phase is computed

$$g_i = \varphi_i + V_{oi} + u_i - pL.$$

The pL arguments corrects for each group p of constituents determined at a particular longitude L other than Greenwich. Thus, p = 1 for diurnal

able 15.—*Equilibrium argument* $(V_0+u)$ *for meridian of Greenwich at beginning of each calendar year*

| Constituent | 1970 | 1971 | 1972 | 1973 | 1974 | 1975 | 1976 | 1977 | 1978 | 1979 | 1980 | 1981 | 1982 | 1983 | 1984 | 1985 | 1986 | 1987 | 1988 | 1989 |
|---|---|---|---|---|---|---|---|---|---|---|---|---|---|---|---|---|---|---|---|---|
| | ° | ° | ° | ° | ° | ° | ° | ° | ° | ° | ° | ° | ° | ° | ° | ° | ° | ° | ° | ° |
| $J_1$ | 270.0 | 1.8 | 93.1 | 197.4 | 286.6 | 14.3 | 100.2 | 198.6 | 281.8 | 4.9 | 89.1 | 188.9 | 276.5 | 5.6 | 95.8 | 201.0 | 292.7 | 24.7 | 116.8 | 222.8 |
| $K_1$ | 13.4 | 15.5 | 17.1 | 19.0 | 19.2 | 18.2 | 16.2 | 11.1 | 10.5 | 6.8 | 3.7 | 2.5 | 1.5 | 1.5 | 2.4 | 4.9 | 6.9 | 9.2 | 11.6 | 14.8 |
| $K_2$ $L_2$ | 207.2 | 211.5 | 214.8 | 218.4 | 218.2 | 215.8 | 211.5 | 207.6 | 200.9 | 191.2 | 188.2 | 185.6 | 183.1 | 182.6 | 184.2 | 189.3 | 193.5 | 198.3 | 203.3 | 210.0 |
| $M_1$ | 262.8 | 60.3 | 245.2 | 81.8 | 282.4 | 99.0 | 276.4 | 99.7 | 297.9 | 130.9 | 310.2 | 116.6 | 313.4 | 159.2 | 350.3 | 135.8 | 334.5 | 188.0 | 25.5 | 166.0 |
| | 155.2 | 48.6 | 307.8 | 234.9 | 158.7 | 51.8 | 302.5 | 198.6 | 135.7 | 41.8 | 291.5 | 170.8 | 87.9 | 30.0 | 291.6 | 171.7 | 82.0 | 31.2 | 299.1 | 179.8 |
| $M_2$ | 165.4 | 266.8 | 8.0 | 84.5 | 185.3 | 285.8 | 26.0 | 101.8 | 201.8 | 301.9 | 42.0 | 117.9 | 218.4 | 319.1 | 60.0 | 136.8 | 238.1 | 339.6 | 81.0 | 158.1 |
| $M_3$ | 68.1 | 40.2 | 11.9 | 306.8 | 277.9 | 248.6 | 219.0 | 152.7 | 122.7 | 92.8 | 63.0 | 356.8 | 327.6 | 298.6 | 270.0 | 205.2 | 177.2 | 149.3 | 121.6 | 57.1 |
| $M_4$ | 330.9 | 173.6 | 15.9 | 169.1 | 10.5 | 211.5 | 52.1 | 203.6 | 43.7 | 243.8 | 84.0 | 235.8 | 76.7 | 278.1 | 120.0 | 273.6 | 116.2 | 319.1 | 162.1 | 316.2 |
| $M_6$ | 136.3 | 80.4 | 23.9 | 253.6 | 195.8 | 137.2 | 78.1 | 305.3 | 245.5 | 185.7 | 126.0 | 353.7 | 295.1 | 237.2 | 180.0 | 50.3 | 354.3 | 298.7 | 243.1 | 114.2 |
| $M_8$ | 301.7 | 347.1 | 31.8 | 338.2 | 21.0 | 63.0 | 104.1 | 47.1 | 87.3 | 127.5 | 168.0 | 111.6 | 153.4 | 196.2 | 240.0 | 187.1 | 232.4 | 278.2 | 321.1 | 272.3 |
| $N_2$ | 270.1 | 282.7 | 295.2 | 270.0 | 282.0 | 293.8 | 305.3 | 279.3 | 290.6 | 301.9 | 313.3 | 287.4 | 299.2 | 311.2 | 323.4 | 298.4 | 311.0 | 323.7 | 336.4 | 311.7 |
| $2N$ | 14.8 | 298.7 | 222.4 | 95.4 | 18.7 | 301.8 | 224.6 | 96.8 | 19.4 | 302.0 | 224.7 | 97.0 | 20.0 | 303.2 | 226.7 | 100.0 | 23.8 | 307.8 | 231.9 | 105.3 |
| $O_1$ | 150.7 | 249.0 | 347.8 | 61.7 | 162.0 | 263.5 | 6.5 | 85.7 | 191.3 | 296.9 | 41.6 | 119.4 | 221.1 | 321.4 | 60.8 | 134.2 | 232.6 | 330.7 | 68.8 | 141.6 |
| $OO$ | 58.7 | 326.4 | 232.6 | 163.9 | 64.6 | 321.1 | 212.6 | 126.5 | 9.8 | 253.0 | 139.2 | 57.5 | 313.6 | 213.9 | 117.6 | 51.0 | 318.5 | 227.0 | 135.6 | 71.2 |
| $P_1$ | 349.8 | 350.0 | 350.2 | 349.5 | 349.7 | 350.0 | 350.2 | 349.5 | 349.7 | 349.9 | 350.2 | 349.4 | 349.7 | 349.9 | 350.2 | 349.4 | 349.6 | 349.9 | 350.1 | 349.4 |
| $Q_1$ | 265.4 | 265.0 | 275.0 | 247.2 | 258.7 | 271.5 | 285.8 | 263.2 | 280.1 | 297.0 | 312.9 | 289.0 | 301.9 | 313.5 | 324.2 | 295.8 | 305.4 | 314.8 | 324.2 | 295.3 |
| $2Q$ | 0.1 | 281.0 | 202.2 | 72.6 | 355.4 | 279.5 | 205.1 | 80.7 | 8.8 | 297.0 | 224.3 | 98.5 | 22.7 | 305.6 | 227.5 | 97.4 | 18.3 | 299.0 | 219.6 | 88.9 |
| $R_2$ | 177.8 | 177.6 | 177.3 | 178.0 | 177.8 | 177.5 | 177.3 | 178.0 | 177.7 | 177.5 | 177.2 | 178.0 | 177.7 | 177.4 | 177.2 | 177.9 | 177.7 | 177.4 | 177.2 | 177.9 |
| $S_1$ | 180.0 | 180.0 | 180.0 | 180.0 | 180.0 | 180.0 | 180.0 | 180.0 | 180.0 | 180.0 | 180.0 | 180.0 | 180.0 | 180.0 | 180.0 | 180.0 | 180.0 | 180.0 | 180.0 | 180.0 |
| $S_2, 4, 6$ | 0.0 | 0.0 | 0.0 | 0.0 | 0.0 | 0.0 | 0.0 | 0.0 | 0.0 | 0.0 | 0.0 | 0.0 | 0.0 | 0.0 | 0.0 | 0.0 | 0.0 | 0.0 | 0.0 | 0.0 |
| $T_2$ | 2.2 | 2.4 | 2.7 | 2.0 | 2.2 | 2.5 | 2.7 | 2.0 | 2.3 | 2.5 | 2.8 | 2.0 | 2.3 | 2.6 | 2.8 | 2.1 | 2.3 | 2.6 | 2.8 | 2.1 |
| $\lambda_2$ | 285.6 | 197.4 | 109.1 | 7.6 | 278.8 | 189.8 | 100.6 | 358.2 | 268.8 | 179.4 | 90.0 | 347.8 | 258.8 | 170.0 | 81.4 | 340.0 | 251.9 | 163.9 | 75.9 | 334.8 |
| $\nu_2$ $M_2$ | 330.0 | 172.1 | 14.0 | 167.0 | 8.4 | 209.7 | 50.7 | 202.8 | 43.6 | 244.4 | 85.3 | 237.6 | 78.8 | 280.2 | 121.9 | 275.1 | 117.2 | 319.4 | 161.6 | 315.0 |
| $P_2$ | 225.3 | 156.1 | 86.8 | 341.5 | 271.7 | 201.7 | 131.4 | 25.3 | 314.9 | 214.4 | 171.0 | 68.0 | 358.0 | 288.2 | 218.6 | 113.5 | 44.3 | 335.2 | 266.2 | 161.4 |
| | 210.6 | 138.4 | 66.6 | 318.7 | 248.4 | 179.1 | 111.9 | 9.2 | 304.3 | 239.4 | 173.6 | 69.6 | 0.7 | 290.5 | 219.4 | 110.9 | 38.8 | 326.4 | 254.0 | 145.0 |
| $MK$ | 178.9 | 282.3 | 25.1 | 103.6 | 204.4 | 301.0 | 42.2 | 115.9 | 212.3 | 308.7 | 45.7 | 120.4 | 219.8 | 320.5 | 62.4 | 141.7 | 245.0 | 348.8 | 92.6 | 172.8 |
| $MK$ $MN$ | 317.4 | 158.1 | 358.8 | 150.0 | 351.4 | 193.3 | 35.9 | 189.4 | 33.2 | 237.0 | 80.4 | 233.3 | 75.3 | 276.6 | 117.6 | 268.6 | 109.3 | 309.9 | 150.5 | 301.4 |
| $MS$ | 75.6 | 189.5 | 303.2 | 354.5 | 107.2 | 219.5 | 331.3 | 21.1 | 132.4 | 243.8 | 355.3 | 45.3 | 157.5 | 242.2 | 23.4 | 75.1 | 189.1 | 303.2 | 57.5 | 109.8 |
| $2SM$ | 165.4 | 266.8 | 8.0 | 81.5 | 185.3 | 285.8 | 26.0 | 101.8 | 201.8 | 301.9 | 42.0 | 117.9 | 218.4 | 319.1 | 60.0 | 136.8 | 238.1 | 339.6 | 81.0 | 158.1 |
| | 194.6 | 93.2 | 352.0 | 275.5 | 171.7 | 74.2 | 334.0 | 258.2 | 158.2 | 58.1 | 318.0 | 242.1 | 141.6 | 40.9 | 300.0 | 223.2 | 121.9 | 20.4 | 279.0 | 201.9 |
| $Mf$ $MSf$ | 44.0 | 308.7 | 212.4 | 141.1 | 41.3 | 298.8 | 193.0 | 110.4 | 359.3 | 248.0 | 138.8 | 59.0 | 316.2 | 216.2 | 118.4 | 48.4 | 313.0 | 218.1 | 123.4 | 54.8 |
| $Mm$ | 191.6 | 93.2 | 352.0 | 275.5 | 174.7 | 74.2 | 334.0 | 258.2 | 158.2 | 58.1 | 318.0 | 242.1 | 141.6 | 40.9 | 300.0 | 223.2 | 121.9 | 20.4 | 279.0 | 201.9 |
| | 255.3 | 344.0 | 72.8 | 174.6 | 263.3 | 352.0 | 80.7 | 182.5 | 271.2 | 0.0 | 88.7 | 190.5 | 279.2 | 7.9 | 96.6 | 198.4 | 287.1 | 15.9 | 104.6 | 206.4 |
| $Sa$ | 280.2 | 280.0 | 279.8 | 280.5 | 280.3 | 280.0 | 279.8 | 280.5 | 280.3 | 280.1 | 279.8 | 280.6 | 280.3 | 280.1 | 279.8 | 280.6 | 280.4 | 280.1 | 279.9 | 280.6 |
| $SSa$ | 200.5 | 200.0 | 199.5 | 201.0 | 200.5 | 200.0 | 199.6 | 201.1 | 200.6 | 200.1 | 199.6 | 201.1 | 200.6 | 200.2 | 199.7 | 201.2 | 200.7 | 200.2 | 199.8 | 201.3 |

(Schureman (1941)'s Table 15)



ble 15.—*Equilibrium argument* $(V_0+u)$ *for meridian of Greenwich at beginning of each calendar year*

| Constituent | 1990 | 1991 | 1992 | 1993 | 1994 | 1995 | 1996 | 1997 | 1998 | 1999 | 2000 |
|---|---|---|---|---|---|---|---|---|---|---|---|
| | ° | ° | ° | ° | ° | ° | ° | ° | ° | ° | ° |
| $J_1$ | 314.4 | 45.2 | 135.2 | 237.9 | 325.0 | 50.2 | 134.0 | 231.1 | 322.5 | 39.3 | 125.8 |
| $K_1$ | 16.7 | 18.0 | 18.7 | 19.4 | 18.0 | 15.6 | 12.2 | 9.5 | 6.0 | 3.2 | 1.5 |
| $K_2$ $L_2$ | 213.9 | 216.6 | 217.6 | 218.5 | 215.4 | 210.3 | 204.0 | 199.2 | 192.7 | 187.2 | 183.4 |
| $M_1$ | 2.2 | 212.4 | 49.0 | 205.8 | 30.4 | 229.4 | 66.7 | 242.7 | 59.3 | 244.2 | 83.7 |
| | 85.9 | 33.5 | 305.0 | 184.1 | 79.3 | 4.9 | 293.5 | 176.9 | 64.8 | 319.9 | 251.4 |
| $M_2$ | 259.4 | 0.5 | 101.3 | 177.6 | 278.0 | 18.2 | 118.3 | 191.0 | 294.0 | 34.2 | 134.5 |
| $M_3$ | 29.1 | 0.7 | 332.0 | 266.4 | 237.0 | 207.3 | 177.4 | 110.9 | 81.0 | 51.3 | 21.8 |
| $M_4$ | 158.7 | 0.9 | 202.7 | 355.2 | 196.0 | 36.4 | 236.6 | 27.9 | 228.0 | 68.4 | 269.1 |
| $M_6$ | 58.1 | 1.4 | 304.0 | 172.8 | 114.0 | 54.6 | 354.9 | 221.9 | 162.1 | 102.6 | 43.6 |
| $M_8$ | 317.5 | 1.9 | 45.3 | 350.3 | 31.9 | 72.8 | 113.2 | 55.8 | 96.1 | 136.8 | 178.1 |
| $N_2$ | 324.3 | 336.7 | 348.8 | 323.3 | 334.9 | 346.4 | 357.8 | 331.7 | 83.0 | 354.5 | 6.1 |
| $2N$ | 29.2 | 312.8 | 236.3 | 108.9 | 31.9 | 314.6 | 237.3 | 109.4 | 32.0 | 314.7 | 237.6 |
| $O_1$ | 240.1 | 339.0 | 78.7 | 154.0 | 256.1 | 359.7 | 104.8 | 185.2 | 290.5 | 34.6 | 137.2 |
| $OO$ | 338.4 | 243.8 | 146.6 | 73.2 | 327.7 | 217.2 | 102.3 | 12.5 | 256.5 | 144.4 | 37.4 |
| $P_1$ | 349.6 | 349.8 | 350.1 | 349.3 | 349.6 | 349.8 | 350.1 | 349.3 | 349.6 | 349.8 | 350.0 |
| $Q_1$ | 305.0 | 315.2 | 326.1 | 299.7 | 313.0 | 327.9 | 344.3 | 322.9 | 339.5 | 354.9 | 8.8 |
| $2Q$ | 9.9 | 291.4 | 213.6 | 85.4 | 10.0 | 296.2 | 223.8 | 100.6 | 28.5 | 315.2 | 240.3 |
| $R_2$ | 177.6 | 177.4 | 177.1 | 177.8 | 177.6 | 177.3 | 177.1 | 177.8 | 177.5 | 177.3 | 177.0 |
| $S_1$ | 180.0 | 180.0 | 180.0 | 180.0 | 180.0 | 180.0 | 180.0 | 180.0 | 180.0 | 180.0 | 180.0 |
| $S_2, 4, 6$ | 0.0 | 0.0 | 0.0 | 0.0 | 0.0 | 0.0 | 0.0 | 0.0 | 0.0 | 0.0 | 0.0 |
| $T_2$ | 2.4 | 2.6 | 2.9 | 2.2 | 2.4 | 2.7 | 2.9 | 2.2 | 2.5 | 2.7 | 3.0 |
| $\lambda_2$ | 246.6 | 158.2 | 69.6 | 327.7 | 238.6 | 149.4 | 60.0 | 317.5 | 228.1 | 138.8 | 49.6 |
| $\nu_2$ $M_2$ | 157.1 | 358.9 | 200.5 | 353.2 | 194.3 | 35.3 | 236.1 | 28.2 | 228.0 | 68.9 | 271.0 |
| $P_2$ | 92.2 | 22.7 | 313.1 | 207.5 | 137.4 | 67.0 | 356.6 | 250.4 | 180.0 | 109.6 | 39.4 |
| | 72.9 | 1.3 | 290.4 | 183.9 | 115.4 | 48.6 | 343.1 | 241.6 | 176.5 | 110.1 | 42.1 |
| $MK$ | 276.0 | 18.5 | 120.0 | 197.0 | 296.0 | 33.8 | 130.5 | 203.4 | 300.0 | 37.4 | 136.0 |
| $MN$ $2MK$ | 142.1 | 342.9 | 184.0 | 335.8 | 177.9 | 20.8 | 224.4 | 18.4 | 222.1 | 65.2 | 267.6 |
| $MS$ | 223.6 | 337.1 | 90.1 | 140.8 | 252.9 | 4.6 | 116.1 | 165.6 | 277.0 | 28.7 | 140.6 |
| $2SM$ | 259.4 | 0.5 | 101.3 | 177.6 | 278.0 | 18.2 | 118.3 | 191.0 | 294.0 | 34.2 | 131.5 |
| | 100.6 | 359.5 | 258.7 | 182.4 | 82.0 | 341.8 | 241.7 | 166.0 | 66.0 | 325.8 | 225.5 |
| $Mf$ $MSf$ | 319.2 | 222.4 | 124.0 | 49.6 | 305.9 | 198.8 | 88.8 | 3.7 | 253.0 | 144.9 | 40.1 |
| $Mm$ | 100.6 | 359.5 | 258.7 | 182.4 | 82.0 | 341.8 | 241.7 | 166.0 | 66.0 | 325.8 | 225.5 |
| | 295.1 | 23.8 | 112.5 | 214.3 | 303.0 | 31.8 | 120.5 | 222.3 | 311.0 | 39.7 | 128.4 |
| $Sa$ | 280.4 | 280.2 | 279.9 | 280.7 | 280.4 | 280.2 | 279.9 | 280.7 | 280.4 | 280.2 | 280.0 |
| $SSa$ | 200.8 | 200.3 | 199.8 | 201.3 | 200.8 | 200.4 | 199.9 | 201.4 | 200.9 | 200.4 | 200.0 |

Table 4.1b V+u for Greenwich at the beginning of years between 1970-2000.

constituents, p = 2 for semidiurnal constituents etc. The sign of L is negative for longitudes east of Greenwich and positive for longitudes west of Greenwich. For Doha, $L \approx -51°$.

Some disadvantages of harmonic analysis should be noted. First of all, the observer has to decide on beforehand what tidal constituents are to be extracted from the record. A check on the proper extraction of tides is investigation of the residual record z(t)

$$z(t) = u(t) - u_h(t)$$

which should reveal overlooked important frequencies. Secondly, no criteria on the preciseness of the estimates ($a_i$ , $\varphi_i$), which obviously should depend on the length of the record and the sampling interval, can be given from the method of least squares. An approximate error on the ($a_i$ , $\varphi_i$) can be computed from z(t), under the (strict) assumption that z(t) is normally distributed (stationary random or white noise process). Then, the respective approximate error reads

$$\Delta a_i \approx \frac{\sqrt{2}\,\upsilon}{\sqrt{M}}$$

$$\Delta \varphi_i \approx \arcsin\left\{\frac{\sqrt{2}\,\upsilon}{\sqrt{M}\,a_i}\right\}$$

where $\upsilon = [1/N \sum_{i=1}^{N} | z_i^2 | \,]^{1/2}$ , the standard deviation of z(t) and M = ½ N-1 with N the number of data points. Only the simplest form of error is given above and it should be kept in mind that in $u_h(t)$ all tidal components should be retained and that even then, z(t) is not a random process under general ocean conditions. The advantage of the method of least squares is that data gaps may exist in the record without preventing the calculations. Data gaps are annoying however, when another (spectral) type of analysis is performed on tides (section 4.2.2). As mentioned in Chapter 1, the residual series z(t) may still contain (internal) tidal motions that can only be removed using band-pass filters (section 4.3).

Assuming that z(t) do not contain tidal or other long wave signals anymore, their relation with other z(t) from different instruments may be determined. They may be subjected to a whole class of statistical methods, of which we only mention the cross correlation function, which describes their mutual relationship as a function of lag k

$$r_{12}(k) = c_{12}(k)/(c_{11}(0)\, c_{22}(0))^{1/2}$$

where $c_{12}(k) = \frac{1}{N} \sum_{i=1}^{N-k} (z_{1,i} - \bar{z}_1)(z_{2,i+k} - \bar{z}_2)$

for series $z_1$ and $z_2$ . The overbar denotes the mean values of the series. At lag 0, $c_{12}(0)$ is called the corariance between two series. It is seen that for totally unrelated series (like white noise) $r_{12}(k) = 0$ for all k, . The $\sigma_1 = c_{11}(0)^{1/2}$ is called

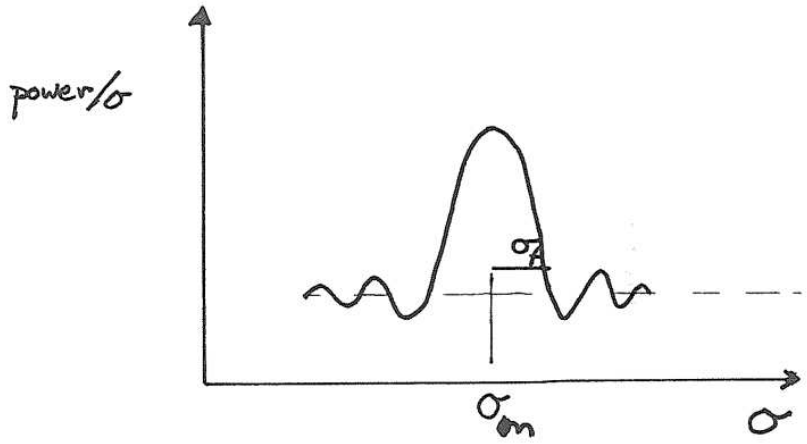
power/σ
σA
σm
σ

Fig 4.4

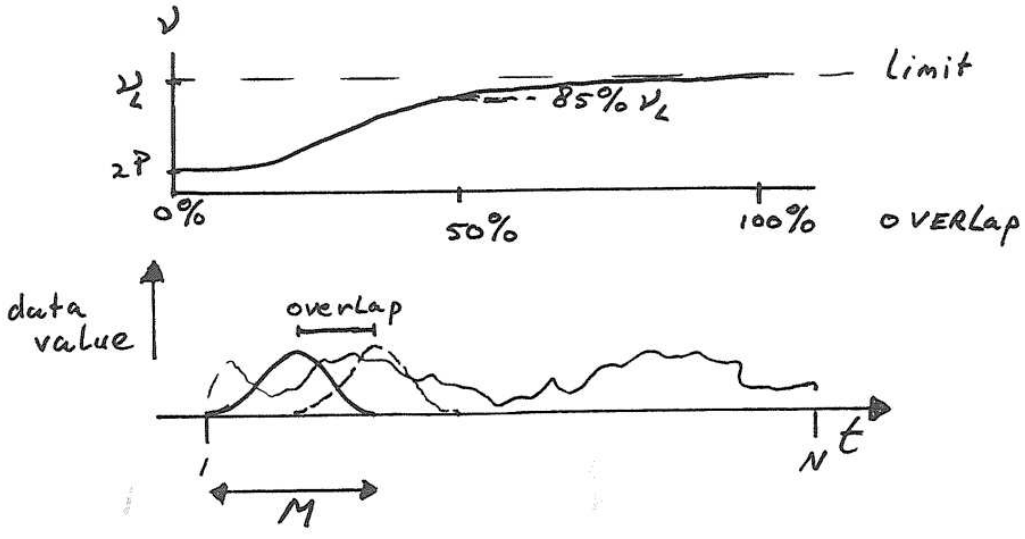
ν
νL
limit
85% νL
2P
0%
50%
100%
OVERLap
data value
overlap
1
N
t
M

Fig 4.5

the standard deviation of a time series $z_1$ and generally referred to as the error of a series. More properly, the 95% confidence limit is used as a measure for the significance of estimates. This limit amounts approximately 1.96 x $\sigma_1$. The standard deviation of a random time series reduces with length N according to

$$\sigma_1 = \sigma_1' / \sqrt{N}$$

where $\sigma_1'$ is the standard deviation of an individual data point.

### 4.2.2 Spectral analysis

Spectral analysis is performed on a representation of a time series as a frequency series. To obtain such representation of the data record, the data have to be transformed from the time domain to the frequency domain, whereby use is made of the relation that a time period $t \propto 1/\sigma$ with $\sigma$ frequency. Under Fourier transform, the time series is represented as a sum of sines and cosines, a Fourier series. For a finite time series of length T, sampled at intervals $\Delta$, so that $N = T/\Delta$ a set of N equations for N unknowns may be constructed in terms of periodic functions

$$u(t) = u_r = A_0 + 2 \sum_{m=1}^{n-1} \{ A_m \cos 2\pi m \sigma_f t + B_m \sin 2\pi m \sigma_f t \} + A_n \cos 2\pi n \sigma_f t$$

with $t = r\Delta$ ($r = -n, \ldots, 0, \ldots, n-1$) and where $\sigma_f = 1/\Delta N$ denotes the fundamental frequency which corresponds to a period equal to the length of the record. The highest frequency present is $n/\Delta N = 1/2\Delta$, the Nyquist frequency.

It is the purpose of Fourier transform to determine the coefficients , $A_m$ , $B_m$ which are a function of (multiples) of the fundamental frequency ($\sigma_m = m/\Delta N$)

$$A_m = \frac{1}{N} \sum_{r=-n}^{n-1} u_r \cos \frac{2\pi m r}{N}$$

$$B_m = \frac{1}{N} \sum_{r=-n}^{n-1} u_r \sin \frac{2\pi m r}{N}$$

which together describe a spectrum. This spectrum consists of an amplitude and phase part

$$R_m = (A_m^2 + B_m^2)^{1/2} \qquad \varphi_m = \arctan (-B_m/A_m)$$

The squared amplitude spectrum of currents components describes the power (kinetic energy) content per frequency band $\sigma_m$ of width $\sigma_f$ (Fig. 4.4). As large energy differences over the frequency range occur in an ocean spectrum, one usually plots log ( $R_m^2$) versus log $\sigma_m$.

Fourier analysis resembles harmonic analysis in that it decomposes into harmonic functions. In Fourier analysis they are a multiple of the fundamental frequency however, whereas in harmonic analysis (known) frequencies are used by the observer. In tidal analysis both methods yield similar results, when a

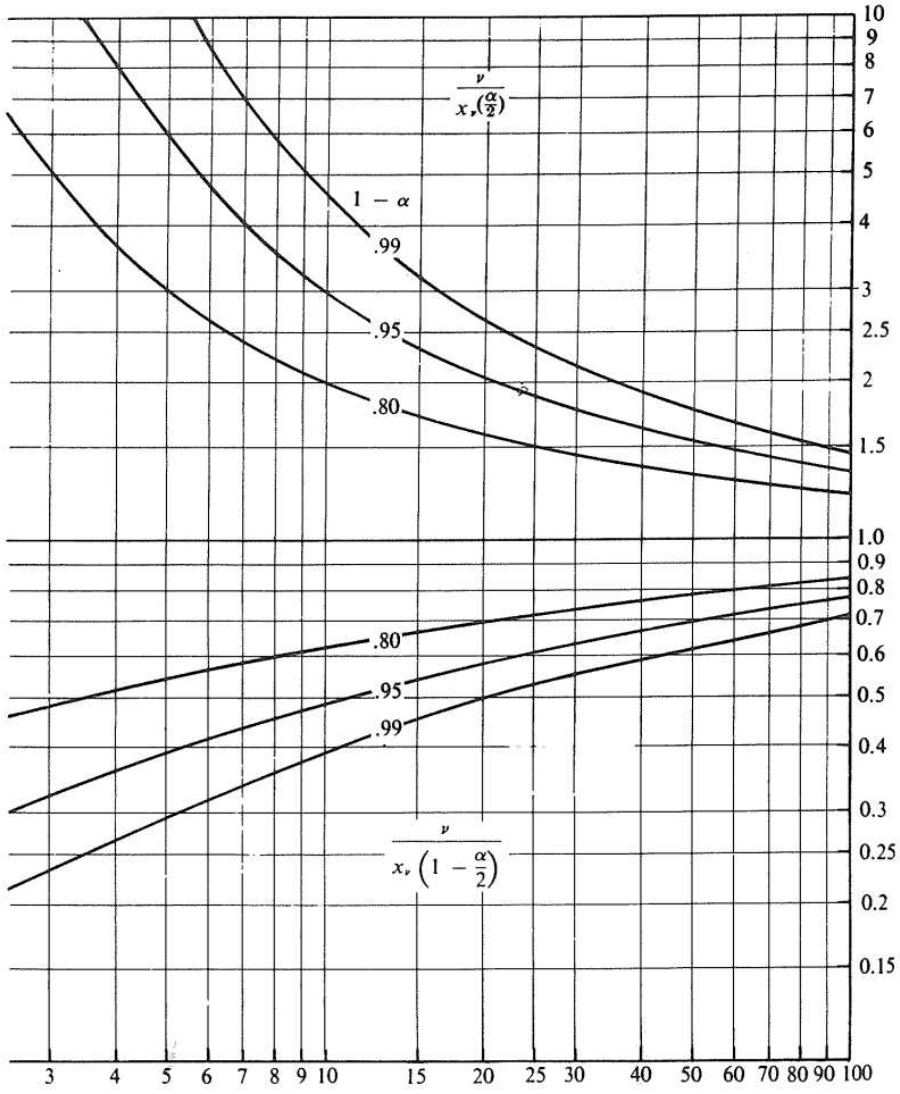


Table 4.2 Plot of $\frac{\nu}{x_\nu(\alpha/2)}$, $\frac{\nu}{x_\nu(1-\alpha/2)}$ vs. $\nu$ for $(1-\alpha) = 0.80, 0.95, 0.99$

multiple of $\sigma_f$ matches the known frequencies or, equivalently, when the record length is a multiple of the tidal period. The advantage of Fourier analysis is that it provides a possibility to compute error bars for the spectral estimates, which are related to the band width or fundamental frequency.

A finite series u (t) can be considered as a sample of a stochastic series, the infinitely long time series. Thus, we want to know what the probability distribution of the estimates in the spectrum are. That is, if we were to repeat the experiment and get a different set of data under similar conditions, how different could the results be? As u(t) is only a single sample of the infinite series, the standard deviation of each spectral estimate in the spectrum, obtained via Fourier analysis over the length of the record is as large as the true value.

In order to decrease the uncertainty of our spectral estimates two possibilities exist. One can split the time series in several smaller series of equal length, Fourier analyse them and average the spectra. This, in fact, means rerunning an experiment of shorter duration several times. One could also, with the same result, average the contents of a number of neighbouring frequency bands, whereby effectively the fundamental frequency increases. For P data pieces, the probability distribution function of the observed spectrum $\Gamma_o = R_m^2$ divided by the time spectrum $\Gamma_t$ reads $\Gamma_o/\Gamma_t = \chi_\upsilon^2/2\upsilon$ which has a mean = 1 and a variance of 1/P. The $\chi_\upsilon^2$ is a standard statistical distribution; the $\upsilon = 2$ P are called degrees of freedom, which are to be determined next.

Clipping the data set in P smaller series of M points effectively means viewing the smaller series through a rectangular window. It is the shape of such window that determines $\upsilon$. A nice scheme for increasing $\upsilon$ is obtained by using a cosine bell time window or multiplying the smaller time series by weights $w(t) - 0.5\ (1 + \cos(2\pi t/M))$. Then still $\upsilon = 2$ P, but this windows allows overlapping of consecutive smaller series. By using 50% overlap we find $\upsilon \approx 3.82$ P - 3.24 (Fig. 4.5). From a table (Table 4.2) or a graph the appropriate $\chi^2$ for a certain confidence interval may be found and the spectral estimates are valid within

$$\log \Gamma_o + \log\left(\frac{\upsilon}{\chi_\upsilon(1-\alpha/2)}\right) \leq \log \Gamma_o \leq \log \Gamma_o + \log\left(\frac{\upsilon}{\chi_\upsilon(\alpha/2)}\right)$$

Sofar we treated only some of the aspects of the computation of a spectrum without going into details. What can we learn from a spectrum? Investigation of a spectral plot reveals energetically dominant frequencies. Tidal currents may dominate, but other periodic signals that do not have a known frequency may show up. Examples are wind driven currents, which may enhance the energy contained in the "synoptic band" (signals with periods of several days) or internal waves, which are found at frequencies $f < \sigma < \left(-\frac{g}{\rho}\frac{\partial \rho}{\partial z}\right)^{1/2}$ (fig. 4.6).

The signature of large ocean eddies can be found at mesoscales (periods of a few weeks).

A comparison between two (or more) time series may result in the computation of the spectral equivalent of the cross correlation function. From the cross spectrum two interesting properties are computed, the coherency and phase

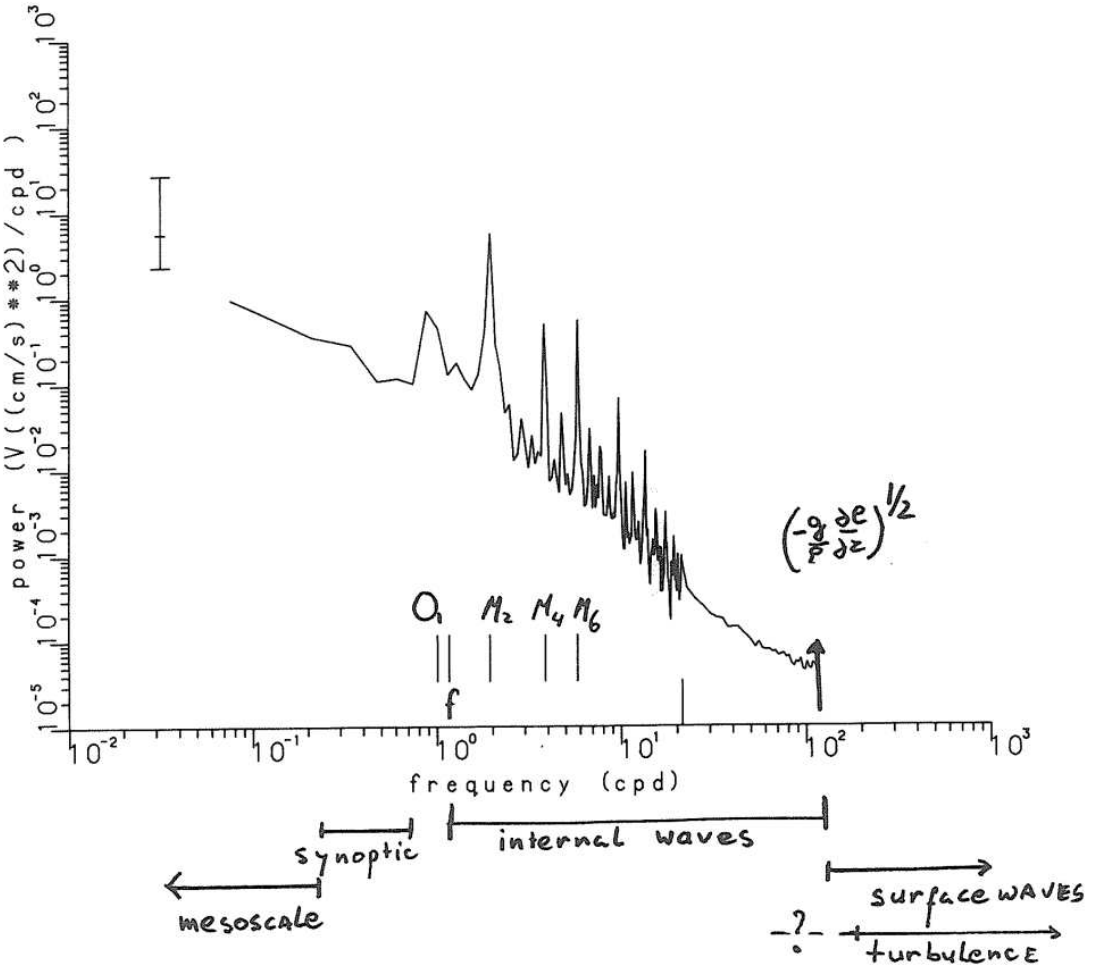


Fig 4.6 Definition of oceanic spectral bands.

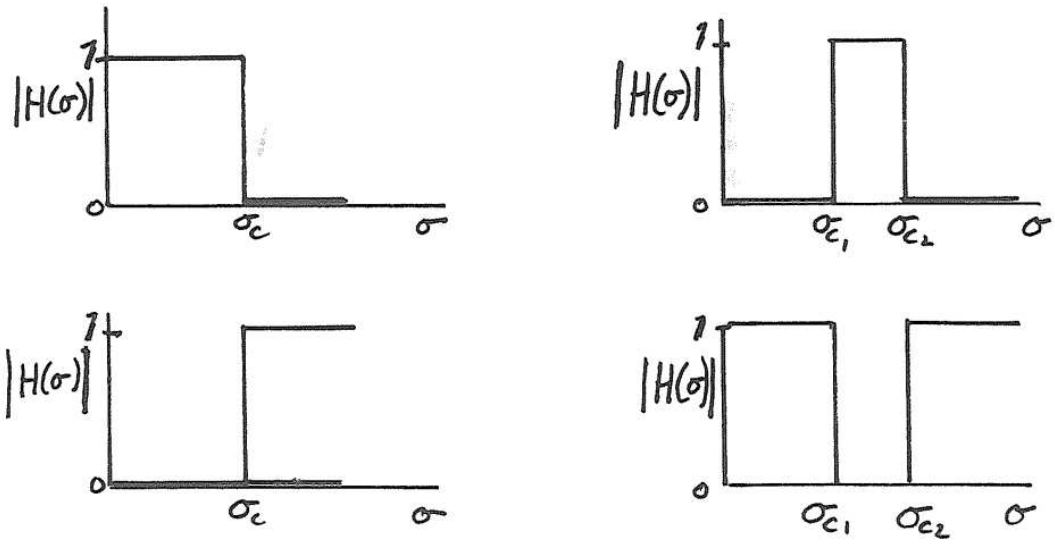


Fig 4.7

spectra, which show the amount of agreement and lag, respectively, between two data records per frequency band.

Visual inspection of the spectrum may lead to the observation of spectral gaps, a number of neighbouring frequency bands that have significantly lower contents than neighbouring spectral peaks. Such gaps are helpful when one wants to separate out part of the signal at specific frequencies, for example for studying the currents driven by the wind. One needs (digital) filters to separate such signals from the total record. It is beyond the scope here to treat this subject fundamentally, but a few notes can be made.

## 4.3 Digital filtering

We already came across the best known filter, the rectangular box. Simply averaging a time series over all or a certain number of neighbouring points, effectively means filtering the data with equal wieghts. Such rectangular filter is not the best filter one can use, although it can suite its purposes under some circumstances. Both analog and digital filters exist, but we concern ourselves with the latter (referred to as "filters"), as we are dealing with discretely sampled data.

Filters are classified according to their response in the frequency domain. A "low-pass" filter leaves unaltered the spectral contents at frequencies lower than a certain cut-off frequency $\sigma_c$, while suppressing signals at $\sigma > \sigma_c$. One could equally design a "high-pass", "band-pass" or, the reciprocal of the latter, a "band-stop" filter (Fig. 4.7).

Filters that use all points of a time series as (only) input are called non-recursive filters. Other names for them are "moving average" and "FIR" (finite impulse response) filters. The advantage of such filters is that they are symmetric and do not distort the phase of the input signal. Generally they are less sharp however, than asymmetric "recursive" filters ("autoregressive" or "infinite impulse response" filters). These use the filter output of previous data as input in a feed back system and are suitable for filtering real-time data, or a time series of which future values are unknown. Such filter distorts phases however and we will continue with symmetric filters as current meters provide a complete record.

The general design of a filter depends on the purpose and the spatial characteristics of the signal to be filtered. If we have a data record $u_n$ containing $n = 1, ..., N$ data points, the filtered series $y_n$ read

$$y_n = \sum_{k=1}^{m} h_k \, (u_{n+k} - u_{n-k}) \qquad \textbf{(4.1)}$$

where the coefficients $h_k$, $k = 1, ...., m$, are called the filter weights that entirely determine the filter. Their representation in the frequency domain is called the transfer function or amplitude response function

$$H(\sigma) = 2 \sum_{k=1}^{m} h_k \cos(2\pi\sigma k\Delta) \qquad \textbf{(4.2)}$$

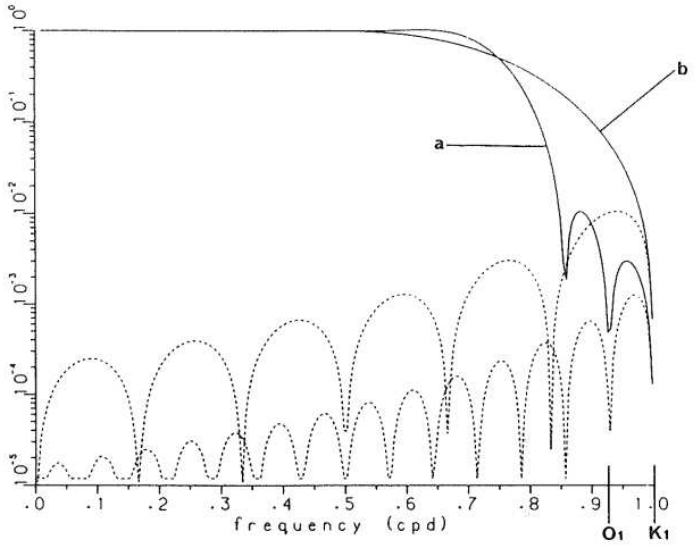


Fig 4.8

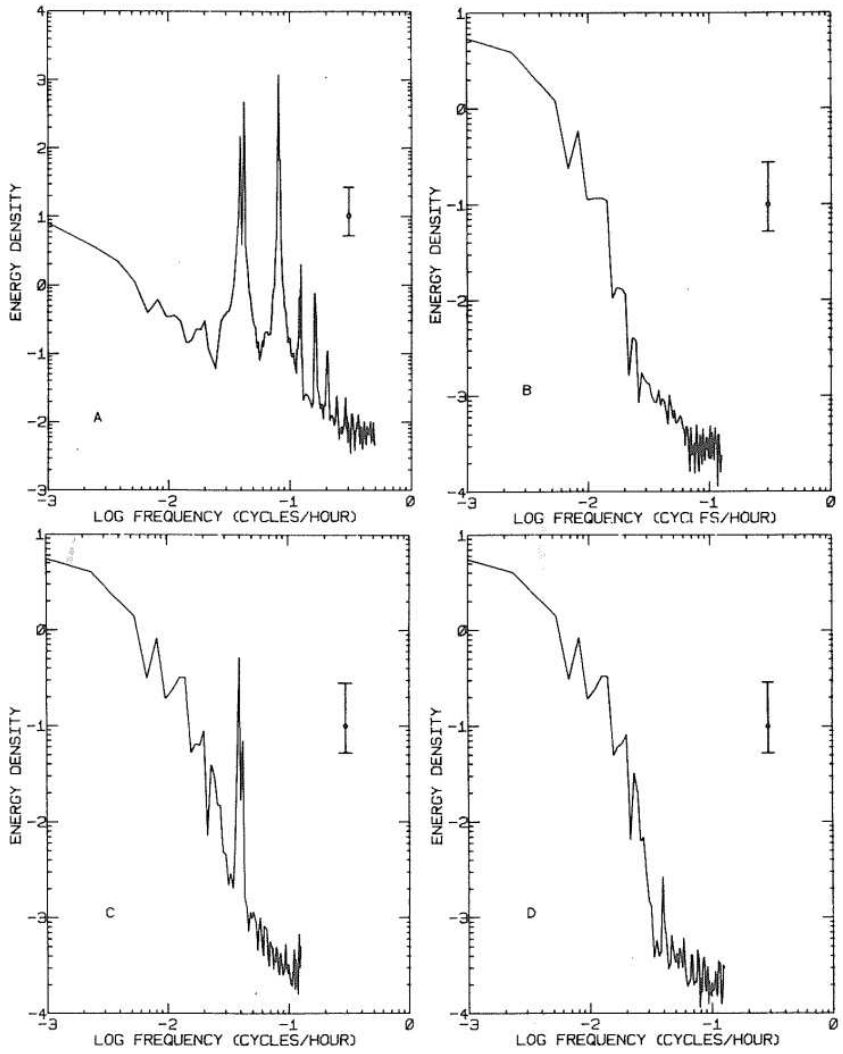


Fig 4.9 A data set (unfiltered in (a)) is filtered at $\sigma_c$=0.025 cph (T=40 hours) by different low-pass filters to remove the tides. Used are: a Godin filter (b), a cosine-Lanczos filter (c) and a cosine-Lanczos squared filter (d).

where $\Delta$ is the sampling interval. The amplitude $|H(\sigma)|$ is the filter gain.

An ideal (low-pass) filter has $|H(\sigma)| = 1$ for $\sigma \leq \sigma_c$ and zero otherwise. The filter weights for such filter are computed by inverting (inverse Fourier transforming) (4.2),

$$h_k = \sin(2\pi\sigma_c(k - M)\Delta)/\pi(k - M)\Delta \qquad 0 \leq k \leq N-1 \qquad \textbf{(4.3)}$$

where $M = (N-1)/2$, but they show a slow decay rate $h_k \propto 1/k$ and only give ideal results for $k \rightarrow \infty$, or an infinite number of weights and hence require an infinitely long time series.

As in the computation of a spectrum, the finite length of a time series to be filtered demands choices between several trade offs. This is where the difficulties of filter design come in. As may be seen from (4.1), a filtered series $y_n$ contains 2m points less than the input series $u_n$. On both ends m points are lost due to filtering. A finite number of weights has the trade off that the filter introducesz sinusoidal motions to the filtered series as may be seen from (4.3). Equivalently a filter of equal weights $h_k$ introduces unwanted ripples in the frequency domain. This "leakage" effectively means that some of the high frequency motions are contained in (leaking into) the filtered low-pass signals.

Specially shaped filters suppress the leakage and hence approach the ideal filter by increasing the power difference between the passing and stopped part of the signals (Fig. 4.8). The frequency range $\sigma_r$ over which the signal is suppressed also depends on the number of weights $\sigma_r \propto 1/m\Delta$. A filter should be designed so that it suppresses unwanted signals at a sufficiently fast rate. As the oceanic spectrum is red, this means that the constraints on a design are heavier for a high-pass filter than for a low-pass filter.

Generally, the better the filter suppresses side lobes , the larger the width of this transition band. An example of different filters is given in Fig. 4.9.

A multi-purpose filter, especially useful for the removal of tides, is the Cartwright filter. It has the following weights for a low-pass version

$$h_k = \cos^2\left(\frac{\pi k\Delta}{2m}\right) \cdot \left[\cos\left(\frac{\pi k\Delta}{2m}\right) - \cos\left((C + \tfrac{1}{2})\,\sigma_N \frac{\pi k\Delta}{m}\right)\right] / \left[2m \sin\left(\frac{\pi k\Delta}{2m}\right)\right]$$

where the cut-off frequency is given by $C\sigma_N/m = C/2\Delta m$ and $\sigma_N$ is the Nyquist frequency. It has the properties

$$|H(\sigma)| = 1 \qquad \sigma < (C-1)/2\Delta m$$

$$|H(\sigma)| = 0 \qquad \sigma < (C+2)/2\Delta m\,.$$